Supporting Information

Engineered Extracellular Vesicle-Based Nanoformulations That Coordinate Neuroinflammation and Immune Homeostasis, Enhancing Parkinson's Disease Therapy

Chuan Zhang[†,a], *Wei Shao*[†,a], *Hao Yuan*[†,a], *Ru Xiao*[a], *Yaru Zhang*[a], *Chaoqi Wei*[a], *Xinyi Ni*[a], *Ning He*[a], *Guangliang Chen*[b], *Shuangying Gui**[,a], *Zhifei Cheng**[,a], *Qi Wang**[,a]

[a]Anhui Province Key Laboratory of Pharmaceutical Preparation Technology and Application, School of Pharmacy, Anhui University of Chinese Medicine, Hefei, Anhui 230012, China.
[b]Department of Integrated Traditional Chinese and Western Medicine, Anhui University of Chinese Medicine, Hefei, Anhui 230012, China.
E-mail: wangqi-njnu@ahtcm.edu.cn (Q. Wang); zfcheng@ahtcm.edu.cn (Z. Cheng); guishy0520@ahtcm.edu.cn (S. Gui)

Experimental Section

Materials

Tetraethyl orthosilicate (TEOS), triethanolamine (TEA), hexadecyltrimethylammonium toluene-p-sulphonate (CTAT), amiloride and methyl-β-cyclodextrin (MβCD) were all purchased from Aladdin Biochemical Technology Co., Ltd. (Shanghai, China). Chlorpromazine (CPZ) was provided from Alta Scientific Co., Ltd. (Tianjin, China). CCL2 inhibitor bindarit was gained from Shandong Sparkjade Biotechnology Co., Ltd. (Shandong,China). Catalase was purchased from Shanghai yuanye Bio-Technology Co., Ltd. (Shanghai, China). $NaBH_4$ was purchased from Sinopharm Chemical Reagent Co.,Ltd. (Shanghai, China). (3-Chloropropyl) Triethoxysilane was purchased from Shanghai Titan Scientific Co., Ltd. (Shanghai, China). 3, 3′-dioctadecyloxacarbocyanine perchlorate (DiO), DCFH-DA and 5, 5′, 6, 6′-Tetrachloro-1, 1′, 3, 3′-tetraethyl-imidacarbocyanineiodide (JC-1) were all purchased from Shanghai Beyotime Biotechnology. (Shanghai, China). 4', 6-diamidino-2-phenylindole (DAPI) and Calcein/PI Live/Dead assay kit were purchased from Beijing Labgic Technology Co., Ltd. (Beijing, China). Dihydrotanshinone I (DT), Cy5 maleimide, 1-methyl-4-phenyl-1, 2, 3, 6-tetrahydropyridine hydrochloride (MPTP) were all provided from Bide Pharmatech co., ltd. (Shanghai, China). Thiazolyl blue tetrazolium bromide (MTT) was obtained from Shanghai Macklin Biochemical Technology Co., Ltd. (Shanghai, China). FerroOrange was obtained from Dojindo Laboratories (Kumamoto, Japan). DMEM (high glucose) and Pen-Strep were purchased from Shanghai Xinyu Biotechnology Co., Ltd. Exosome depleted fetal bovine serum was obtained from Shanghai XP Biomed Ltd. (Shanghai, China).

Instrumentation

The shape of different samples was analyzed by transmission electron microscopy (TEM, (Hitachi HT7800, JEOL Ltd., Japan). The material was dropped into a 200-mesh copper grids and stained with 2% phosphotungstic acid (If it was required to stain). The diameter and the particle number of different samples were detected by Nanoparticle Tracking Analysis (NTA) software (NanoSight NS 300, Malvern Instruments). Each group was analyzed in triplicates with 30 s per analysis at 25°C. The zeta potentials of different samples were recorded by dynamic light scattering (DLS, ZEN3690, Malvern, USA). The materials at a concentration of 0.2 mg mL^{-1} in a PBS buffer was prepared for DLS analysis. The ^{1}H-NMR spectra of DSPE-PEG_{2000}-Mal, DSPE-PEG_{2000}-MG1 and BTESePD were recorded on the Bruker ADVANCE III 600 MHz spectrometer. All fluorescence images of cells were captured by CLSM (Olympus FV3000, Japan) and Inverted fluorescence microscope (LEICA DMI8, Germany). Evaluation of cell polarization, detection of intracellular Fe and investigation of mitochondrial dysfunction were tested on flow cytometry (BD FACSCelesta). Cell viability and brain cytokines was detected by Microplate reader (SpectraMax i3X, USA). The *in vivo* and *ex vivo* biodistribution were carried out on *in vivo* imaging system (IVIS, PerkinElmer).

Cell lines and animals

MSC, BV2, bEnd.3 cells and SH-SY5Y cell line were purchased from the Shanghai Xinyu Biotechnology Co., Ltd (shanghai, China), RAW 264.7 cells was purchased from BNCC, and cultured in DMEM culture medium containing 10% of FBS and 1% of Pen/Strep/Amp solution at 37℃ in a 5% CO_2 humidified incubator. C57BL/6 mice were purchased from Hangzhou Ziyuan Experimental Animal Technology Co., Ltc. (Hangzhou, China). All *in vivo* experiments were approved by the Animal Welfare Committee of Anhui University of Chinese Medicine (Hefei, China, AHUCM-mouse-2024016).

Isolation of MSC^{CCR2} EVs

First, MSC stably expressing the chemokine receptor CCR2 was constructed by genetically engineered method[1]. Briefly, MSC cells (5×10^5 cells $well^{-1}$) were seeded and cultured in a 6-well plate for 24 h. Then 100 μL of lentivirus solution (10^9 TU mL^{-1}) was added to each well, and further incubated at 37℃ for 6 h. Subsequently, the culture medium containing lentivirus was replaced with fresh mouse bone marrow mesenchymal stem cell culture medium (containing 10% FBS, 1% Pen-Strep (v/v) and 1% Glutamine) and continue to culture for 48~72 h to obtain MSC^{CCR2} stably expressing the chemokine receptor CCR2.

Then MSC^{CCR2} were seeded into the T25 cell culture flask with mouse bone marrow mesenchymal stem cell culture medium (containing 10% FBS, 1% Pen-Strep (v/v) and 1% Glutamine. When the cell density reached 70% in the culture flask, the cells were transferred to the T75 culture flask for further incubation for 24h. Then the culture medium was replaced with EV-depleted medium (among then, 10% FBS was replaced with 1% exosome-free serum in the above medium). After 24 h of incubation, the culture medium was collected and stored at -80℃ until use.

And finally, the above culture medium was centrifuged for 30 min by 2000 rpm and 10000 rpm at 4 ℃, respectively. After removing dead cells and cell fragments, the supernatant was further centrifuged by 100000 rpm for 120 min at 4℃ (DiO (0.5 mL, 20 μM) or Cy5 (0.5 mL,1 mg mL^{-1}) was added when stained), and the lower MSC^{CCR2} EVs was resuspend in PBS by discarding the supernatant. MSC EVs was extracted using similar procedures as described above except for replacement with MSC without transfection.

To precisely target microglia with M1 phenotype, MG1 peptide was prepared using solid phase synthesis technology and further modified on the surface of MSC^{CCR2} EVs according to previously reported literature[2]. 10 mg of MG1 peptide and 10 mg of DSPE-PEG_{2000}-Mal were dissolved in 2 mL of DMF under N_2 atmosphere in dark for 96 h. After dialysis by deionized water and freeze drying, 10.0 mg of product was mixed with 100 μL of MSC^{CCR2} EVs (the density of 10^9 particle mL^{-1}) for 24 h in the dark at 4℃.

Protein quantification of MSC^{CCR2} EVs and EVN

100 μL of MSC^{CCR2} EVs and EVN were added into 100 μL of lysate, respectively. The sample was broken by ultrasonic crusher for 30 s (5 times), then placed on ice and incubated for 30 min. The above sample was centrifuged and collected for 5 min by 12000 g at 4 ℃. Then the supernatant was taken as total protein extract, and the protein was quantified by BCA kit (Beyotime).

Preparation of MSeN-DT

The biodegradable MSeN-DT was synthesized by three steps according to previous reports[3]. Firstly, Bis [3-(triethoxysilyl) propyl] diselenide (BTESePD) containing diselenide-bond as organosilica precursor was synthesized as follows. 0.9 g of $NaBH_4$ was dissolved into 12 ml of deionized water at room temperature. Then, 1.92 g of Se powder was added slowly into the above solution within 5 min, followed by stirring at 70°C for 20 min to obtain Na_2Se_2. After adding dropwise 4.2 mL of (3-chloropropyl)-triethoxysilane, the mixture was stirred at 50℃ for 12 h in the dark. The reaction was stopped by ice water, and further extracted three times with dichloromethane and concentrated using a rotary evaporator. The final product namely BTESePD was purified by column chromatography.

Secondly, the biodegradable MSeN was co-condensed through a modified sol-gel method using TEOS as inorganic silicon source and BTESePD as organosilica precursors. Briefly, 0.3 g of CTAT (dispersed in 20 mL of deionized water) were mixed

with 64 μL of TEA and stirred at 80°C for 30 min. Then, 1.0 g of TEOS was dropped into the mixture solution for kept with 1 h. A mixture containing 3.0 g of TEOS and 0.5 g of BTESePD was injected dropwise and stirred for 3 h. Next, the finally product (named as MSeN) was washed three times with ethanol, and refluxed for 12 h at 80℃in an ethanol solution (containing 1% of NH_4NO_3, W/V) to remove template.

Finally, to load effectively drug, DT was dissolved in ethanol by sonication to obtain a stock solution (5 mg mL^{-1}). Then, 12.5 mg of MSeN was resuspended in 2.5 mL of ethanol, followed by adding 2.5 mL of DT solution (5 mg mL^{-1}). The above solution was mixed at 200 rpm for 24 h in dark, and further washed by ethanol to obtain the product (named as MSeN-DT). To detect the release of DT, 20 mg of MSeN-DT was re-dispersed in the mixture (PBS/ethanol = 7/3, V/V) with 0 or 100 μM H_2O_2, and shaken at 200 rpm at 37 °C. Then, the above solution was centrifuged to collect the supernatant for detection at preset time points.

Degradation of MSeN

8 mg of MSeN (100 μg·mL^{-1}) was dispersed into PBS with or without 100 μM of H_2O_2 at 37 °C. Samples were collected at 0, 1, 3 and 5 days for TEM observation.

Western blot for CCR2 and CD63 on EVN

100 μL of MSC^{CCR2} EVs and MSC EVs and EVN was dispersed with 100 μL of lysis buffer, respectively. After shaking violently at 4℃ for 30 s, the above solution was incubated on ice for 4 min (repeated for 5 times). After then lysed and centrifuged (12,000 g, 5 min), the supernatant was obtained as whole protein extract for determination by a BCA protein assay kit (Jiangsu KeyGEN BioTECH Corp., Ltd, KGA902). Next, 30 μg of proteins were run through an SDS-PAGE and then transferred onto PVDF membranes. subsequently, the PVDF membranes were blocked with blocking buffer and probed with Rabbit Anti-CCR2 (1:1000; Affinity Biosciences Cat#DF2711), Rabbit Anti-CD63 (1:1000; Affinity Biosciences Cat#AF5117) followed by HRP-conjugated secondary antibodies at 1:2000 dilution at room temperature for 1 h. Finally, protein signals were detected by ECL reagents and analyzed by Gel-Pro32 with GAPDH normalization.

Detection of the content of CCL2

10 ng mL^{-1} of CCL2 protein (5 μL) was incubated with MSC^{CCR2} EVs, MSeN-DT and EVN (500 μL, the density of 10^6 particle mL^{-1}) for 2 h. Then, the mixtures were centrifuged by 15,000 g for 30 min at 4 °C for examination by ELISA kit. Besides, the binding capacity with CCL2 of EVN at different times (0, 2, 4, 8 and 12 h) was used with the similar methods as described above.

Cell viability assays

BV2 cells (1×10^4 cells $well^{-1}$) were seeded and cultured in a 96-well plate for 24 h. If the stimulus treatment was requested, a final concentration of 100 μM of H_2O_2 was added and further incubated at 37 ℃ for 24 h. Further, EVN at different concentration was added and incubated with the BV2 cells for 24 h in triplicate. Then, the BV2 cells were washed and added by 20 μL of MTT (5 mg mL^{-1}) for incubation for 4 h at 37 ℃. Cell viability was detected by the absorbance at 490 nm by the microplate reader. In addition, similar experimental steps were used for cell viability except for replacing different concentrations or different incubation times with different samples.

Live/dead staining was further applied to investigate the cell viability. Similar procedures as described above were used to obtain cells treated with different samples. Then, the treated cells were stained with Calcein-AM (2 mM, labeled the surviving cells) and PI (1 mg mL^{-1}, labeled the dead cells) for 20 min. Then the cells were washed with PBS and observed by fluorescence microscope.

Determination of intracellular ROS

Typically, BV2 cells (5×10^4 cells mL^{-1}) were seeded into the culture dish and cultured for overnight. If the stimulus treatment was requested, a final concentration of 100 μM of H_2O_2 was added and further incubated at 37℃ for 24 h. Further, different samples (MSC^{CCR2} EVs, MSeN-DT and EVN, 10^6 particle mL^{-1}) was added and incubated for 24 h in triplicate. After then, the BV2 cells were washed and stained with 2 μM of DCFH-DA for 30 min. The treated cells were observed by fluorescence microscopy or collected into flow tube for detection of fluorescence intensity.

Cellular uptake

BV2 cells (5×10^4 cells mL^{-1}) were seeded into the culture dishes for overnight. If the stimulus treatment was requested, a final concentration of 100 μM of H_2O_2 was added and further incubated at 37℃ for 24 h. After then, Cy5 labeled different sample at a final concentration of 10^6 particle mL^{-1} was added and co-cultured with different time (1 h, 2 h and 4 h). Subsequently, the treated BV2 cells were washed, stained for 15 min (10 μM of DiO, 5 μg mL^{-1} of DAPI). After washing gently with PBS, the fluorescence images of BV2 cells were collected with fluorescence microscope.

To investigate the targeting efficiency of EVN to different types of cells, BV2 cells and SH-SY5Y cells (5×10^4 cells mL^{-1}) were seeded into the culture dishes for overnight. IL-4 (20 ng mL^{-1}) was added into BV2 cells, and SH-SY5Y cells were added with H_2O_2 (100 μM), and further incubated at 37℃ for 24 h. After then, Cy5-labeled EVN at a final concentration of 10^6 particle mL^{-1} was added and co-cultured with 4 h. Finally, each cells were washed with PBS and collected into flow tube for detection of fluorescence intensity.

Endocytosis pathway detection

BV2 cells (1×10^6 cells mL^{-1}) were incubated in a 6-well plate at 37℃. After 12h, cells were pre-incubated at 4°C for 1 hour, and then the different samples (MSC^{CCR2} EVs, MSeN-DT and EVN, 10^6 particle mL^{-1}) were added and cultured for 4h. Next, to investigate the effects of endocytosis inhibitors, cells were pretreated at 37°C for 2 hour with the following specified concentrations of endocytosis inhibitors: 10 μg mL^{-1} of clathrin-mediated endocytosis inhibitor chlorpromazine (CPZ); 500 μM of caveolin-mediatedendocytosis inhibitor methyl-β-cyclodextrin (MβCD); 1 mM of macropinocytosis inhibitor amiloride were added and incubated for 2 h. After then, the different samples (MSC^{CCR2} EVs, MSeN-DT and EVN, 10^6 particle mL^{-1}) were added and incubated for another 4h. Finally, BV2 cells were harvest after being washed with PBS and the signal of sampls were detected by flow cytometer.

Besides, FRET detection was used to verify membrane fusion. Typically, A pair of fluorescent dyes (Dil and DiD) was co-labeled into EVN, following by adding the increasing numbers of BV2 cells. Then, the fluorescence spectrum (550 nm-750 nm) was used to detected at an excitation wavelength of 525 nm.

Western blot of BV2 cells

BV2 cells were seeded in 6-well plates at a density of 5×10^5. After 24 h, H_2O_2 (100 μM) was added for 24 h to establish an inflammatory microglia model. After being washed twice with PBS, the cells were treated with 1 mL medium containing PBS, and MSC^{CCR2} EVs, MSeN-DT, EVN respectively, for 24 h, and then collected and resuspended with 100 μL of lysis buffer. After the protein concentration was determined by a BCA protein assay kit (*Jiangsu KeyGEN BioTECH Corp., Ltd*, KGA902), 30 μg of proteins were run through an SDS-PAGE and then transferred onto PVDF membranes. Next, membranes were blocked with blocking buffer and probed with Rabbit Anti-Nrf2 (1:2000; PTG,16396-1-AP), Mouse Anti-GPX4 (1:1000; PTG,67763-1-ig) followed by HRP–conjugated secondary antibodies at 1:2000 dilution at room temperature for 1 h. Last, protein signals were detected by ECL reagents and analyzed by Gel-Pro32 with GAPDH normalization.

Flow cytometry analysis

(1) Evaluation of cell polarization *in vitro*

The polarization of microglia was detected by fluorescence staining (CD86 represented M1 phenotype, CD206 represented M2 phenotype). BV2 cells (1×10^6 cells mL^{-1}) were incubated in a 6-well plate for overnight. If the stimulus treatment was requested, a final concentration of 100 μM of H_2O_2 was added and further incubated at 37℃ for 24 h. After then treated with different samples (1×10^6 particles mL^{-1}) for 24 h, BV2 cells were digested and washed by centrifugation with PBS. Then, the cells were treated by fixation/permeabilization buffer (BD Biosciences, 554722) for incubation with 20 min, and perm/wash buffer (BD Biosciences, 554723) for incubation with 15 min. Subsequently, BV2 cells were collected and labeled with FITC-CD86 (PTG, FITC-65068) and PE-CD206 (Biolegend, 141705) antibodies. After washing with flow cytometry staining buffer, the resuspended cells were immediately detected by the flow cytometer.

(2) Flow cytometry analysis *in vivo*

Mice in each group were euthanized with an overdose of isoflurane and were immediately taken by cardiac perfusion with pre-cooled saline. The midbrain of mice in each group was isolated and minced sufficiently to completely immerse in 2 mL of digestion solution (DMEM containing 1 mg mL^{-1} of collagenase IV and 20 U mL^{-1} of DNAase I). The above mixture was digested at 37 ℃ for 30 min. After then, the digestion reaction was terminated by adding complete medium to the above lysates, and a 40 μM cell filter was further used to remove insufficiently digested tissue blocks and cell masses, resulting in a brain tissue suspension.

For detecting polarization of microglia of the midbrain of mice in each group (CD86 represented M1 phenotype, CD206 represented M2 phenotype, TMEM119 represented microglia). After, the cells were washed gently with flow cytometry staining buffer and then treated by fixation/permeabilization buffer (BD Biosciences, 554722) for incubation with 20 min, and perm/wash buffer (BD Biosciences, 554723) for incubation with 15 min. Subsequently, BV2 cells were collected and labeled with FITC-CD86 (PTG, FITC-65068), PE-CD206 (Biolegend, 141705) and TMEM119 (PTG, 27585-1-AP) antibodies. Flow cytometer was used for analysis.

To investigate the infiltration of macrophage cells ($CD45^{high}$ CD^{11b+}) at 24 h after tail injection of different samples in mice, density gradient centrifugation was performed to isolate inflammatory cells from single-cell suspensions using 30-70% Percoll (Beijing Labgic Technology Co., Ltd). Monocyte cells were collected from the interface between 30% percoll and 70% percoll and washed twice with PBS. Subsequently, the monocyte cells were labeled with FITC-CD11b (PTG, FITC-65055), PE-CD45

(PTG, PE-65087) antibodies. Flow cytometer was used for analysis.

(3) Detection of intracellular Fe

BV2 cells (1×10^5 cells mL^{-1}) were seeded and cultured in the culture dish for overnight. If the stimulus treatment was requested, a final concentration of 100 μM of H_2O_2 was added and incubated at 37℃ for 24 h. And BV2 cells were pretreated with a ferroptosis inhibitor (DFO, 100 μM) for 1 h. Next, different samples (MSC^{CCR2} EVs, MSeN-DT and EVN, 10^6 particle mL^{-1}) were added and incubated for 24 h in triplicate. After then, the treated cells were washed and stained with 1 μM of FerroOrange reagent for 30 min in the dark. The treated cells were observed by fluorescence microscopy or collected into flow tube for detection of fluorescence intensity.

(4) Investigation of mitochondrial dysfunction *in vitro*

The ability to repair mitochondrial dysfunction of BV2 treated by different samples was observed by mitochondrial membrane potential staining. BV2 cells (5×10^4 cells mL^{-1}) were seeded in the 6-well plate for kept with overnight. If the stimulus treatment was requested, a final concentration of 100 μM of H_2O_2 was added and further incubated at 37℃ for 24 h. Then, different samples (10^6 particle mL^{-1}) were added and incubated for 24 h in triplicate. After treatment, the cells in sequence were washed with PBS, incubated with JC-1 probe (500 μL, 10 μg mL^{-1}) for 30 min. Finally, the fluorescence signal (JC-1 monomers were green, JC-1 aggregates were red) of cells was observed using flow cytometer.

BBB penetration *in vitro*

The BBB model *in vitro* was built according to previously published literature[4]. The bEnd.3 cells were first seeded and cultured for 10 day in the upper chamber of transwell model (0.4 μm of pore size). After the formation of the BBB layer, the BV2 cells were seeded at the bottom of the 24-well plates with H_2O_2 (a final concentration of 100 μM) for 24 h. Next, Cy5 labeled-different samples (10^6 particle mL^{-1}) were added into the upper chamber for 24 h incubation. After discarding the culture medium, the cells in the lower and upper chambers were collected and were stained with DiO (10 μM) for 15 min and DAPI (5 μg mL^{-1}) for 10 min, respectively. The stained BV2 cells were recorded by fluorescence microscope and IVIS imaging system. Penetration rate (%) = Fluorescence intensity of Cy5 from the lower chambers /Fluorescence intensity of Cy5 from the lower chambers and the upper chamber × 100%.

Measurement of protein in BV2

BV2 cells were seeded in 12-well plates at a density of 5×10^4 for overnight. If stimulation treatment was required, a final concentration of 100 μM of H_2O_2 was added and further incubated at 37℃ for 24 h. Furthermore, BV2 cells were treated with the Nrf2 agonist tBHQ (10 μM) and the Nrf2 inhibitor ML385 (10 μM) for 1 h before stimulation with H_2O_2. After then, the cells were treated with MSC^{CCR2} EVs, MSeN-DT, EVN for 24 h respectively. Finally, PKC-δ,GSK-3β、Fyn、GPX4 and Nrf2 were detected by an assay kit (*Jiangsu Meimian Industrial Co., Ltd*).

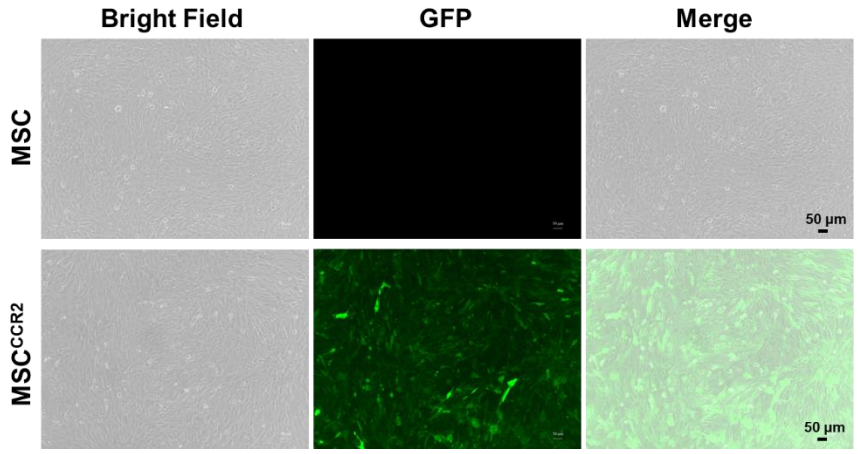

Figure S1. Fluorescence images of normal MSC and transfected MSC cells with GFP expression.

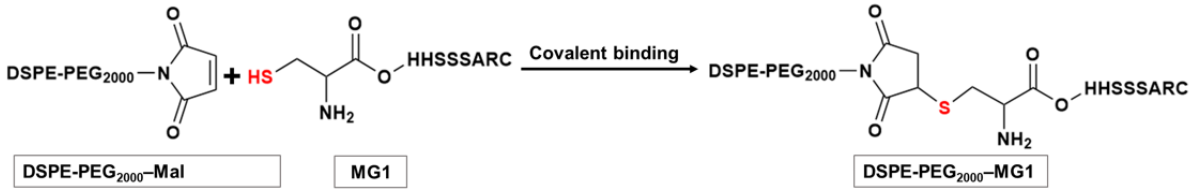

Figure S2. The synthetic process for DSPE-PEG$_{2000}$-MG1.

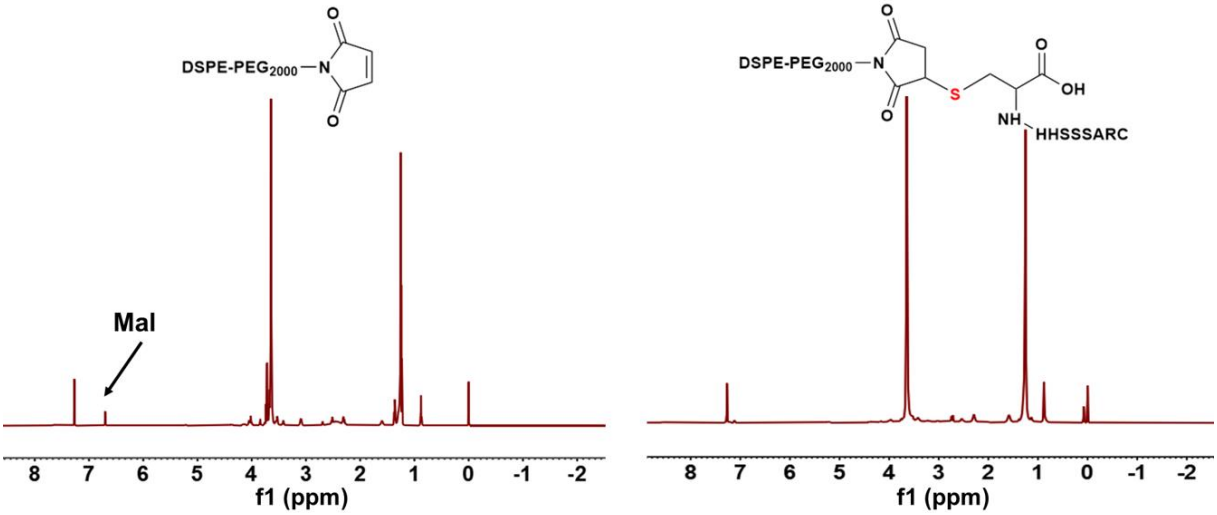

Figure S3. ^{1}H NMR Spectrum of DSPE-PEG$_{2000}$-Mal (left) and DSPE-PEG$_{2000}$-MG1 (right).

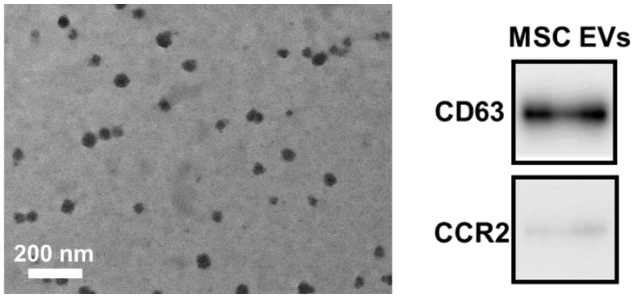

Figure S4. TEM image and WB assay of CD63 and CCR2 expression of MSC EVs.

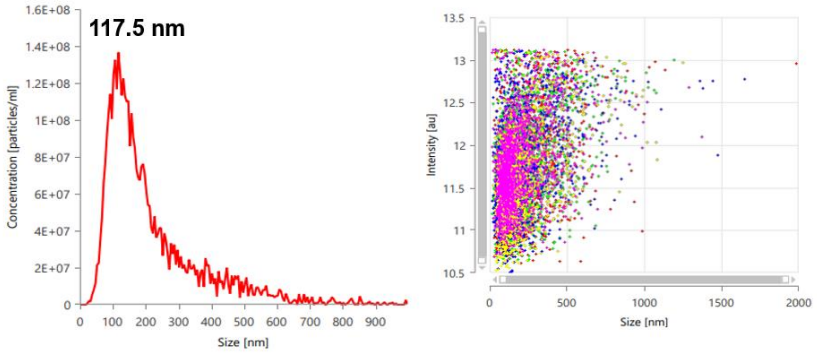

Figure S5. Size distribution of MSC^{CCR2} EVs from NTA. The averaged nanoparticle concentration/size (left). Intensity/size graph for experiment from NTA (right).

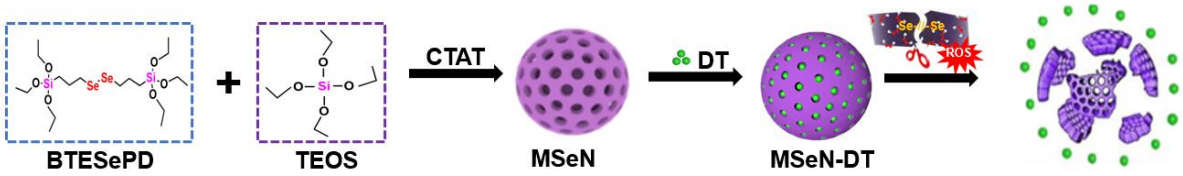

Figure S6. Schematic of fabrication of diselenide-bond-bridged MSeN-DT for ROS-responsive drug release.

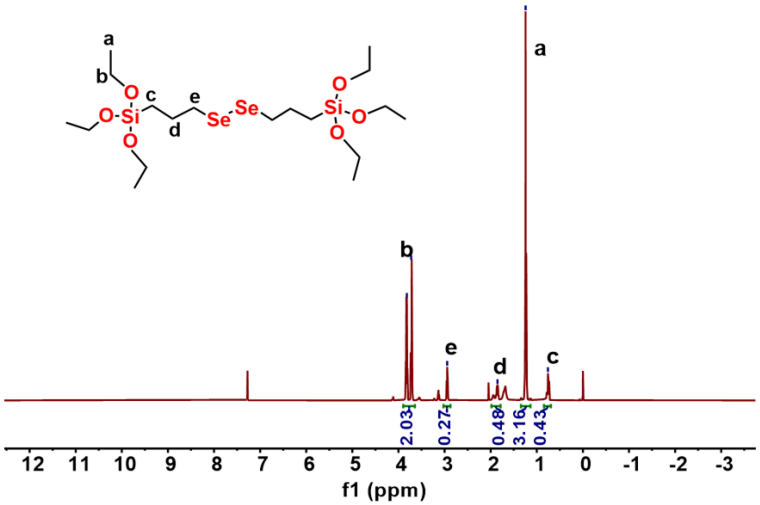

Figure S7. ^{1}H NMR Spectrum of BTESePD.

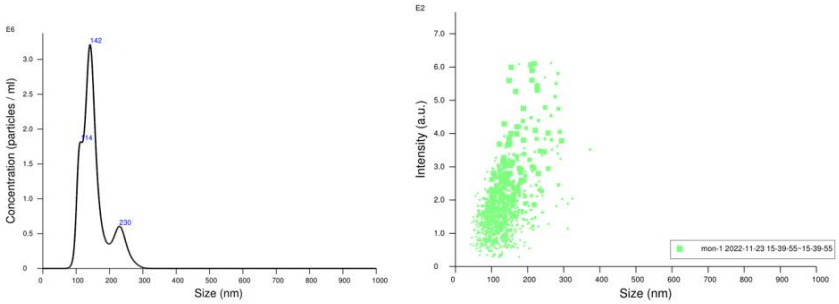

Figure S8. Size distribution of MSeN from NTA. The averaged nanoparticle concentration/size (left). Intensity/size graph for experiment from NTA (right).

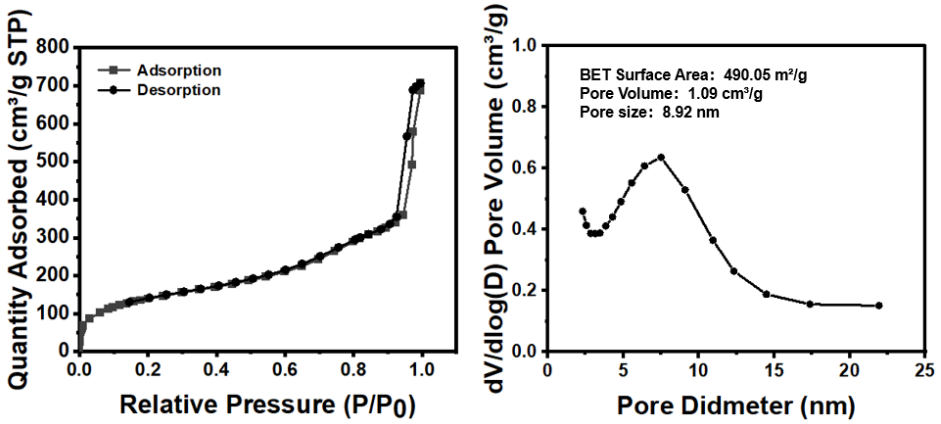

Figure S9. N_2 sorption isotherms (left) and pore size distribution of MSeNs (right).

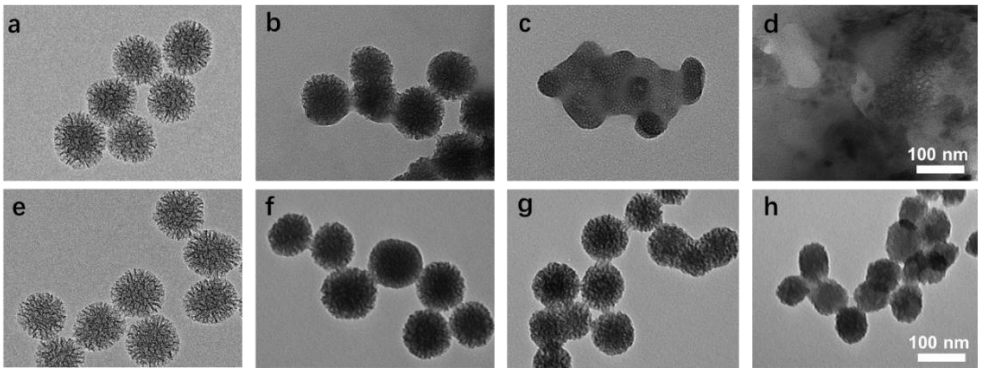

Figure S10. Representative TEM images of MSeNs under PBS containing 100 μM H_2O_2 at 0 d (a), 1 d (b), 3 d (c), and 5 d (d); TEM images of MSeNs under PBS containing 0 μM H_2O_2 at 0 d (e), 1 d (f), 3 d (g), and 5 d (h).

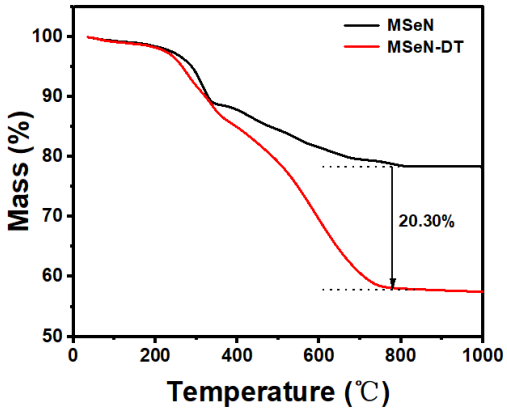

Figure S11. Thermogravimetric analysis (TGA) of MSeN and MSeN-DT.

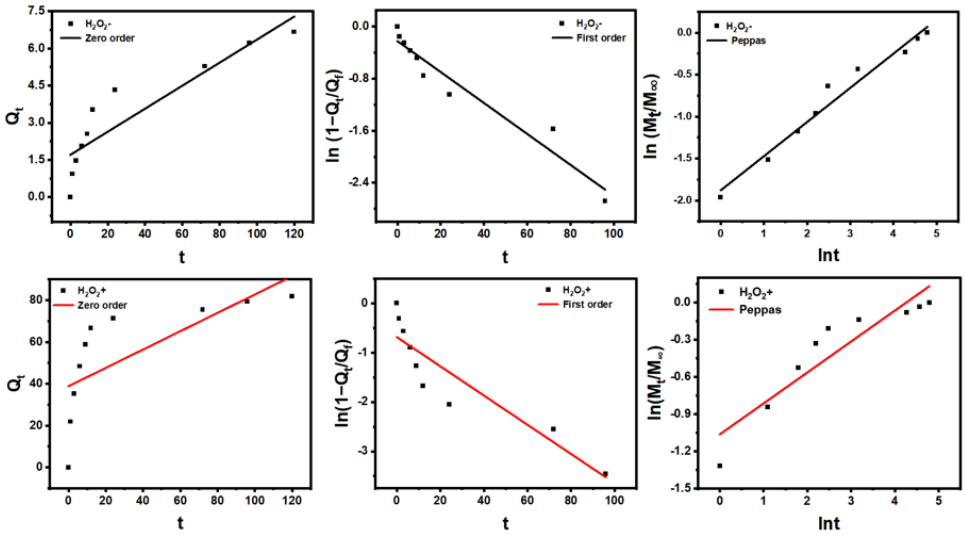

Figure S12. The release kinetics of DT from MSeN-DT under PBS without H_2O_2 (H_2O_2-) and with H_2O_2 (H_2O_2+) for 120 h.

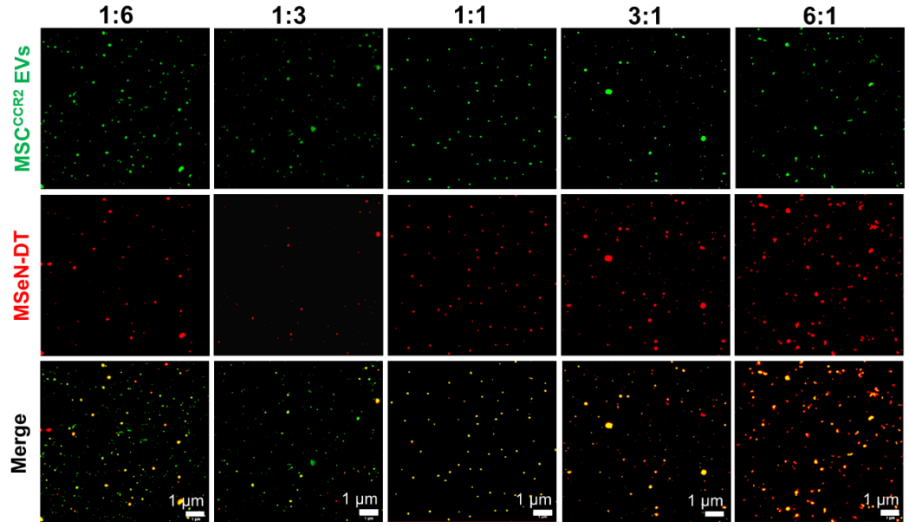

Figure S13. Fluorescence images of EVN with different number ratios of MSeN-DT: MSC^{CCR2} EVs (the red fluorescence represents MSeN-DT; the green fluorescence represents MSC^{CCR2} EVs).

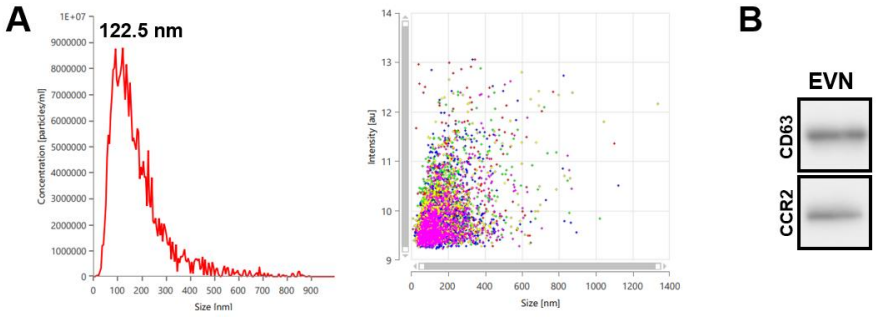

Figure S14. (A) Size distribution of EVN from NTA. The averaged nanoparticle concentration/size (left). Intensity/size graph for experiment from NTA (right). (B) WB assay of CD63 and CCR2 expression in EVN.

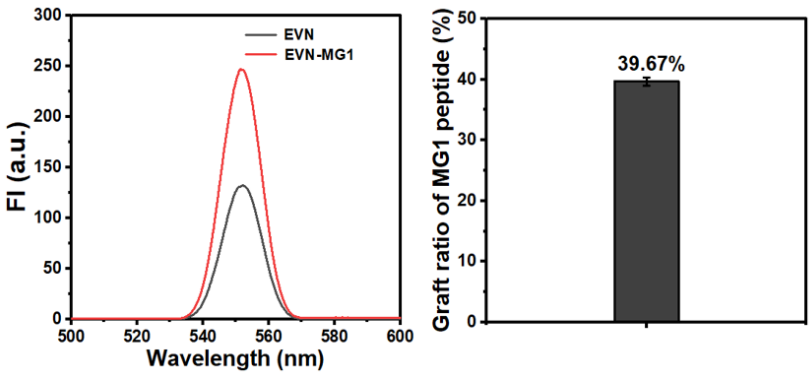

Figure S15. Fluorescence intensity (FI) of Rhodamine B-labeled MG1 peptide on different samples (left) and the corresponding grafting ratio of MG1 peptide (right, n = 3). All statistical data are presented as mean ± standard deviation.

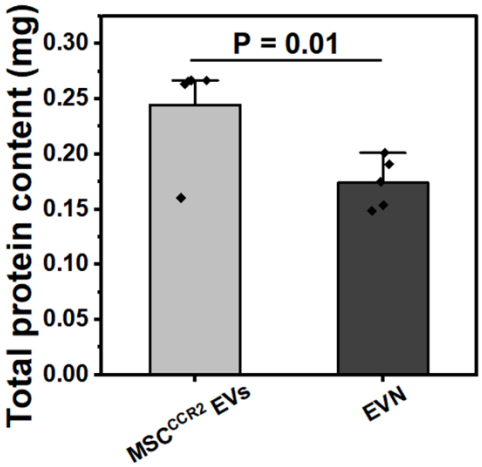

Figure S16. The quantification of total protein content in MSC^{CCR2} EVs and EVN by BCA kit (n = 5). All statistical data are presented as mean ± standard deviation. Statistical analysis: one-way ANOVA followed by Tukey's HSD post hoc test.

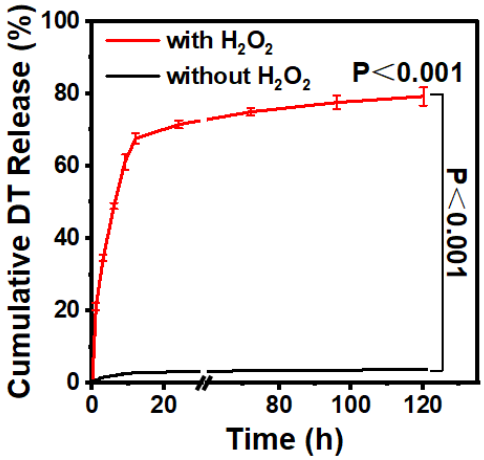

Figure S17. DT release profiles of EVN without and with 100 μM H_2O_2. (n = 3). Statistical analysis: two-way ANOVA followed by Tukey's multiple comparisons post test.

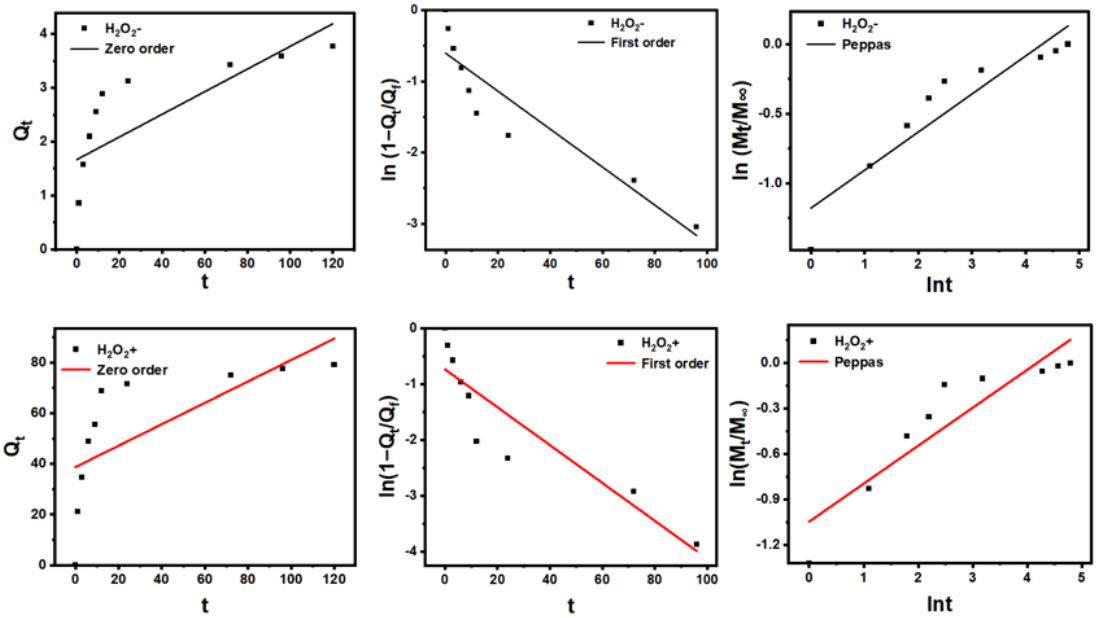

Figure S18. The release kinetics of DT from EVN under PBS without (H_2O_2-) and with 100 μM H_2O_2 (H_2O_2+) for 120 h.

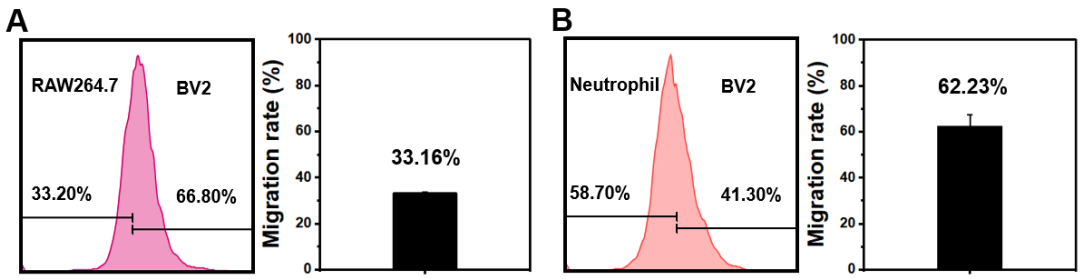

Figure S19. Flow cytometric analysis of (A) the migrated RAW 264.7 and (B) the migrated neutrophils treated by MSC EVs@MSeN-DT through a membrane having an 8-μm pore size with H_2O_2 pre-treated BV2 cells adding CCL2, and the corresponding of quantitative analysis (n = 3). All statistical data are presented as mean ± standard deviation.

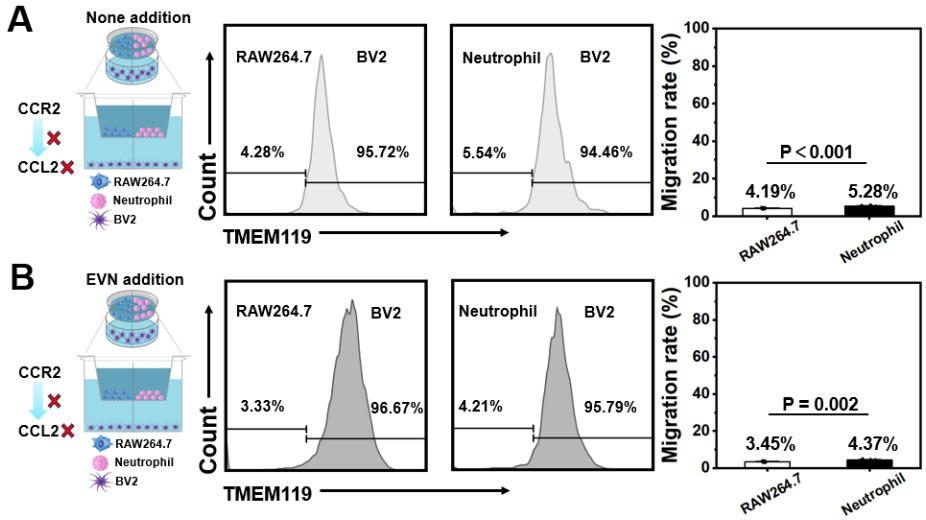

Figure S20. Flow cytometric analysis of the migrated RAW 264.7 and neutrophils through a membrane having an 8-μm pore size under H_2O_2 and CCL2 inhibitor pre-treated BV2 cells (A) without and (B) with EVN, and the corresponding of quantitative

analysis. (n = 3). All statistical data are presented as mean ± standard deviation. Statistical analysis: one-way ANOVA followed by Tukey's HSD post hoc test.

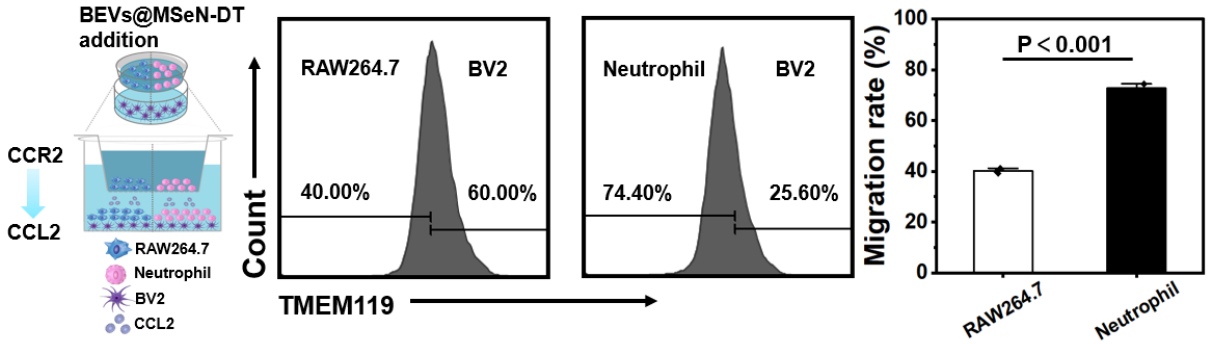

Figure S21. Flow cytometric analysis of the migrated RAW 264.7 and neutrophils through a membrane having an 8-μm pore size under H_2O_2 pre-treated BV2 cells with BEVs@MSeN-DT, and the corresponding of quantitative analysis. (n = 3). All statistical data are presented as mean ± standard deviation. Statistical analysis: one-way ANOVA followed by Tukey's HSD post hoc test.

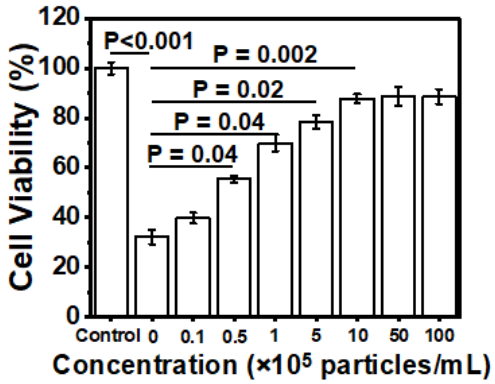

Figure S22. The cell viability of the stimulated BV2 cells treated by different concentrations of EVN (n = 3). All statistical data are presented as mean ± standard deviation. Statistical analysis: one-way ANOVA followed by Tukey's HSD post hoc test.

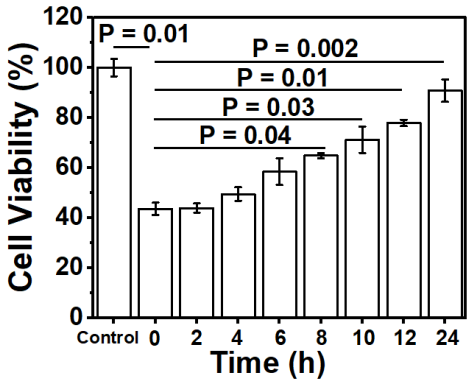

Figure S23. The cell viability of the stimulated BV2 cells treated by EVN at different incubation times (n = 3). All statistical data are presented as mean ± standard deviation. Statistical analysis: one-way ANOVA followed by Tukey's HSD post hoc test.

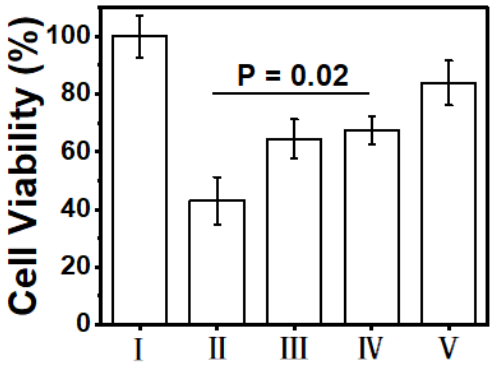

Figure S24. The cell viability of the BV2 cells treated by different samples (n = 3). Ⅰ: Control; Ⅱ: Model; Ⅲ: MSC^{CCR2} EVs; Ⅳ: MSeN-DT; Ⅴ: EVN. All statistical data are presented as mean ± standard deviation. Statistical analysis: one-way ANOVA followed by Tukey's HSD post hoc test.

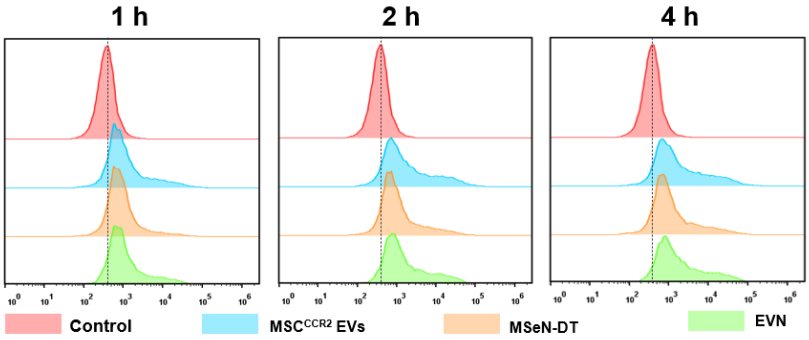

Figure S25. Flow cytometric analysis of the stimulated BV2 cells treated by different samples at different incubation times.

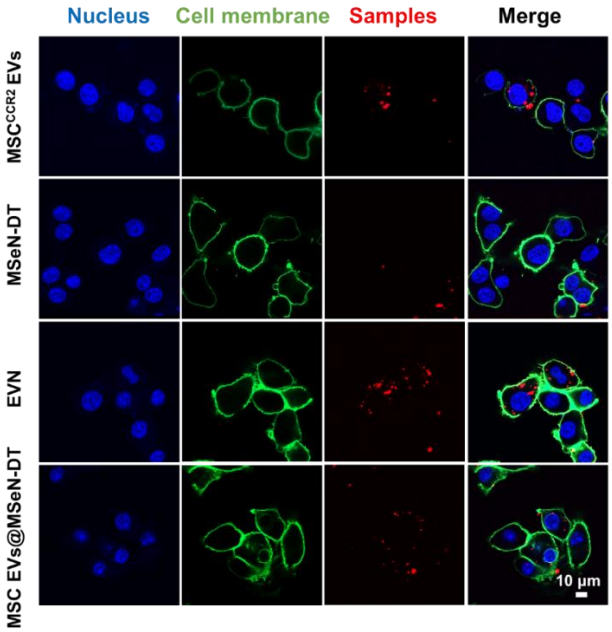

Figure S26. Representative CLSM images of the stimulated BV2 cells after treated by different samples (red: samples, blue: nucleus, green: cell membrane)

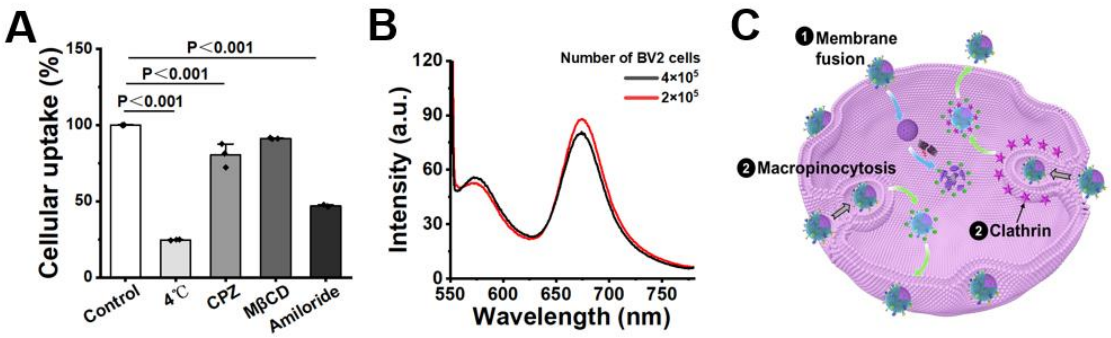

Figure S27. (A) The uptake mechanism of EVN under different condition (n = 3). (B) EVN membrane labeled with fluorescent dyes (Dil and DiD) and fused with increasing numbers of BV2 cells. (C) Schematic illustrating the two main uptake pathways of EVN may correspond to the two release forms of DT in BV2 cells: 1) Endocytosis pathways (clathrin and macropinocytosis), in which EVN releases DT after entering the cell as an intact structure (the DT release profiles of EVN); 2) Membrane fusion pathways: the exposed MSeN-DT entered the cell for DT release (the DT release profiles of MSeN-DT) under the co-fusion between the EVN and BV2 cells. All statistical data are presented as mean ± standard deviation. Statistical analysis: one-way ANOVA followed by Tukey's HSD post hoc test.

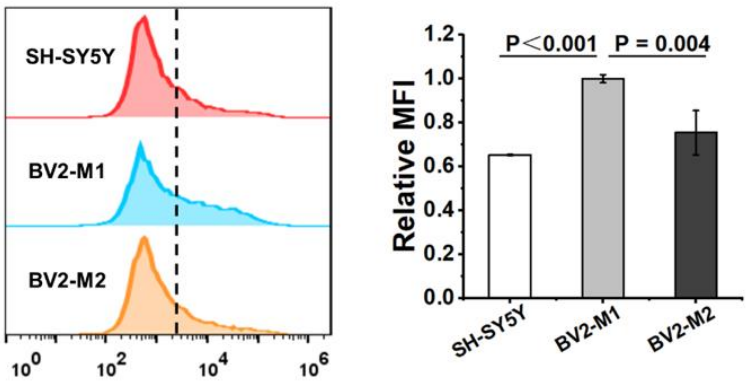

Figure S28. Flow cytometric analysis (left) and relative MFI (right) of SH-SY5Y, M2 phenotype BV2 (BV2-M2) and M1 phenotype BV2 (BV2-M2) treated by Cy5 labeled EVN after 4 h incubation (in which the relative MFI for the BV2-M2 group was denoted as 1, n = 3). All statistical data are presented as mean ± standard deviation. Statistical analysis: one-way ANOVA followed by Tukey's HSD post hoc test.

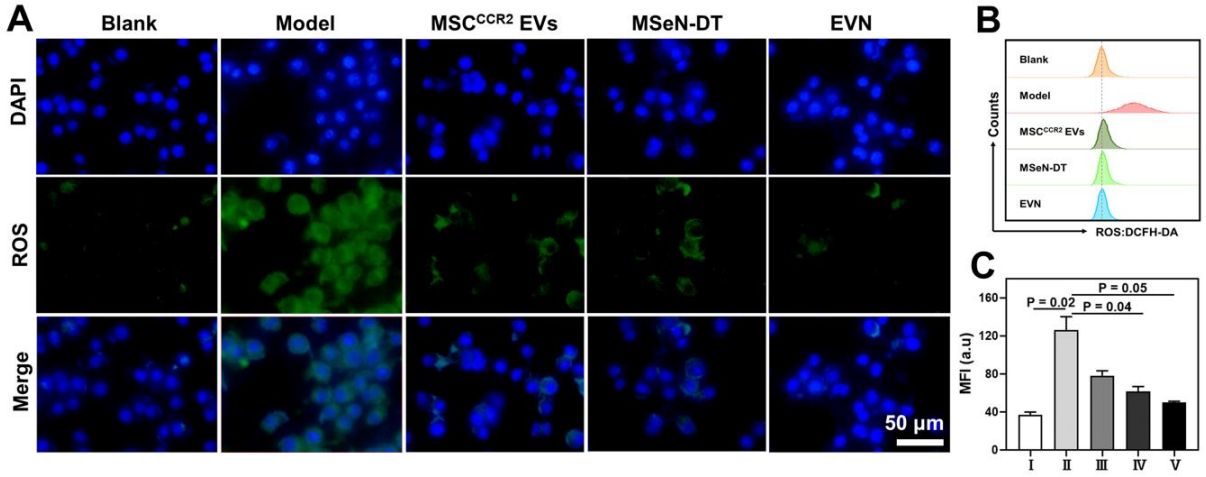

Figure S29. (A) Representative fluorescent images of BV2 cells treated with different samples (green: ROS fluorescence probe, blue: nucleus). Blank group represent BV2 cells without the stimulated treatment, model and other group represent BV2 cells with the stimulated treatment and different samples. (B) Flow cytometry was used to detect the elimination of ROS in BV2 cells stained with ROS fluorescent probes treated with different samples (Ⅰ: Blank; Ⅱ: Model; Ⅲ: MSC^{CCR2} EVs; Ⅳ: MSeN-DT; Ⅴ: EVN). (C) The mean fluorescence intensity (MFI) of ROS in the blank group was recorded as 1 (n = 3). All statistical data are presented as mean ± standard deviation. Statistical analysis: one-way ANOVA followed by Tukey's HSD post hoc test.

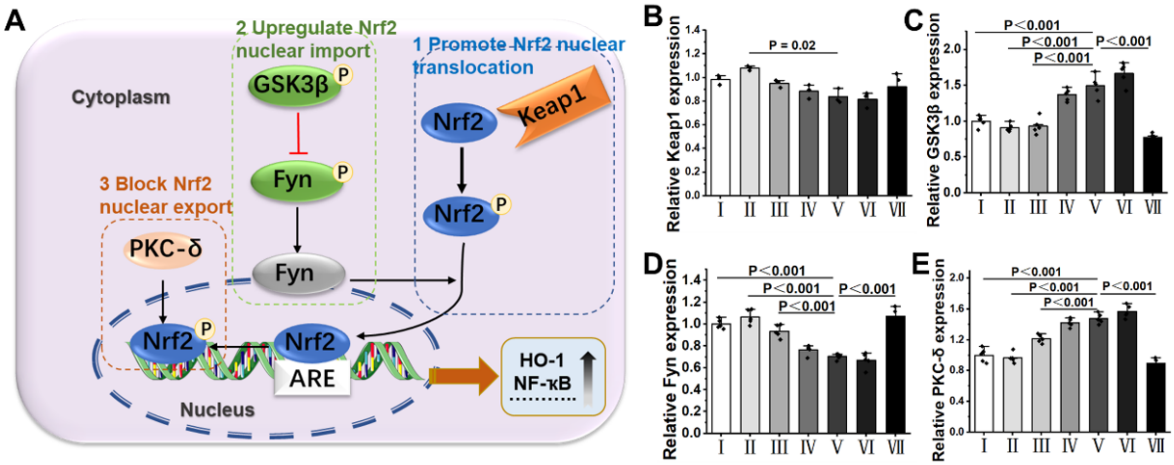

Figure S30. (A) Schematic illustration on mechanism of Nrf2 regulation by DT throughout the process. (B-E) Relative quantification of Keap1, GSK3β, Fyn and PKC-δ in BV2 cells under different conditions, in which the expression of control group as denoted as 1 (I: Control, II: Model, III: MSC^{CCR2} EVs, IV: MSeN-DT, Ⅴ: EVN, Ⅵ: tBHQ, Ⅶ: ML385, n = 3-5). All statistical data are presented as mean ± standard deviation. Statistical analysis: one-way ANOVA followed by Tukey's HSD post hoc test.

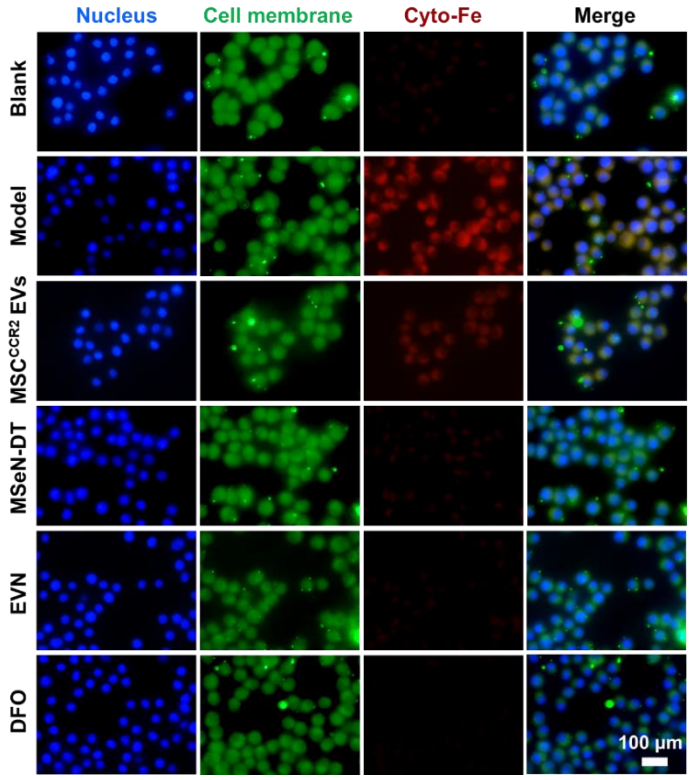

Figure S31. Representative fluorescent images of stimulated BV2 cells after uptake of different samples (blue: nucleus, green: cell membrane, red: Cyto-Fe).

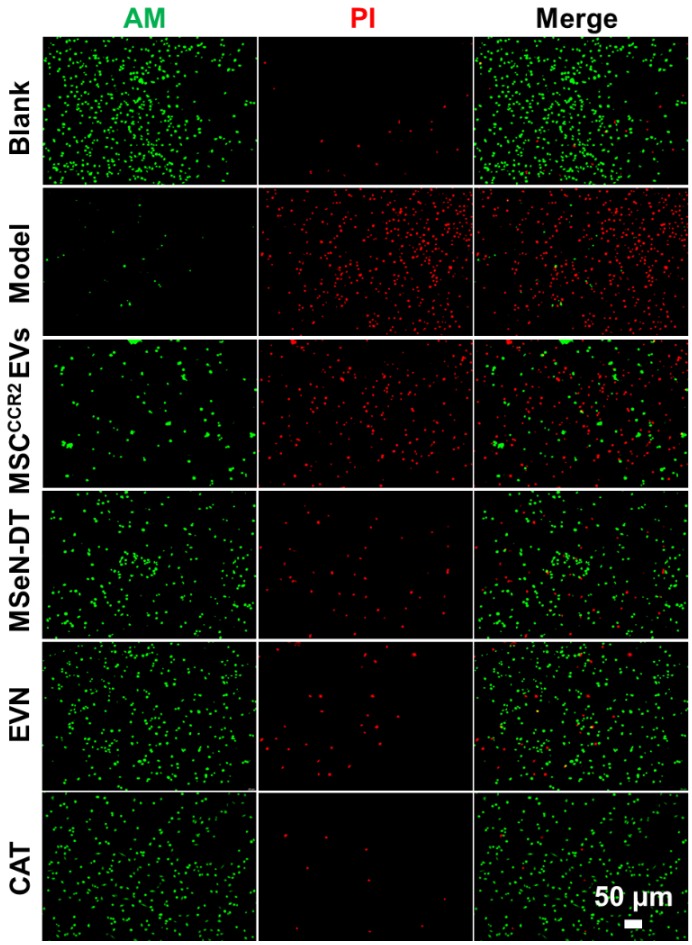

Figure S32. Representative fluorescent images of live&dead staining for SH-SY5Y cells receiving different treatments ((The red fluorescence of PI probe represents dead cells, and the green fluorescence of AM probe represents live cells).

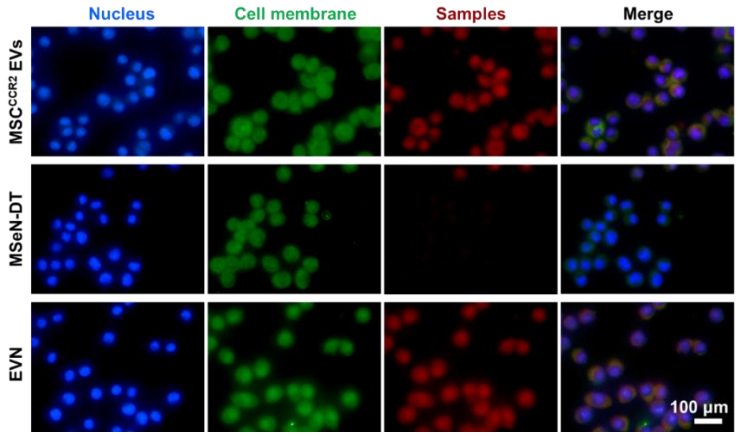

Figure S33. Representative fluorescent images of different samples in the stimulated BV2 cells *in vitro* BBB model (Blue: nucleus, green: cell membrane, red: Cy5-labeled samples).

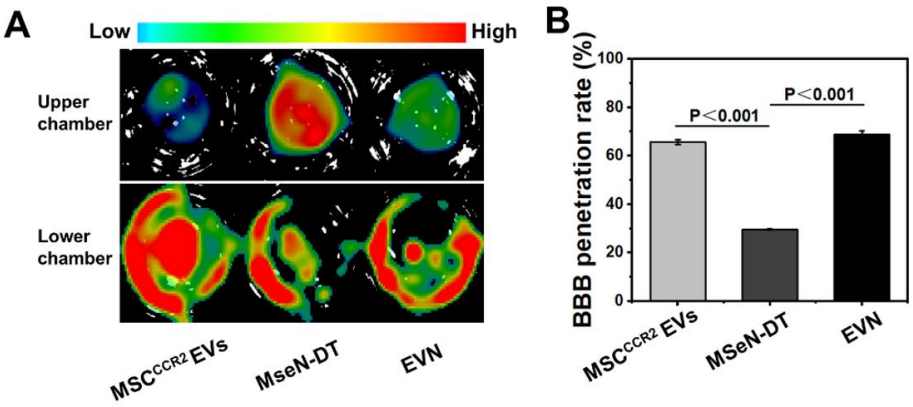

Figure S34. (A) Fluorescence images of the upper chamber and lower chambers incubation of different Cy5 labeled-samples using an in vivo imaging system. (B) BBB penetration rate of different Cy5 labeled-samples (n = 3). All statistical data are presented as mean ± standard deviation. Statistical analysis: one-way ANOVA followed by Tukey's HSD post hoc test.

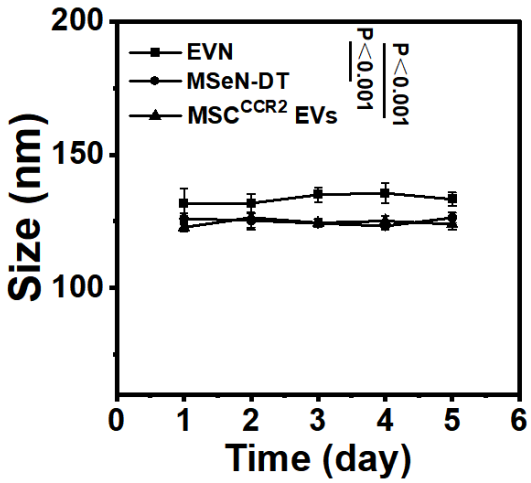

Figure S35. The size of different samples during different incubation times with serum (n = 3). Statistical analysis: two-way ANOVA followed by Tukey's multiple comparisons post test.

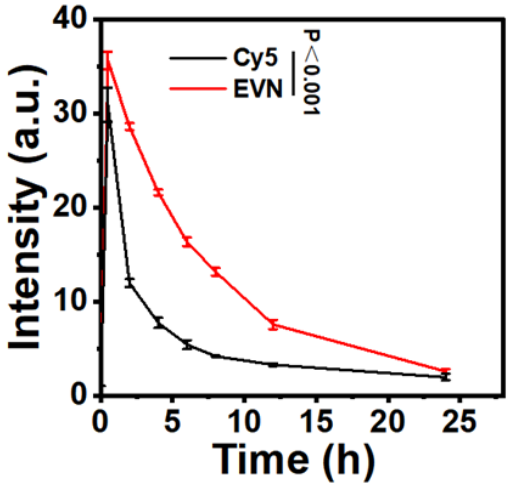

Figure S36. Blood retention of free-Cy5 and Cy5-EVN in rats by single intravenous injection (n = 3). Statistical analysis: two-way ANOVA followed by Tukey's multiple comparisons post test.

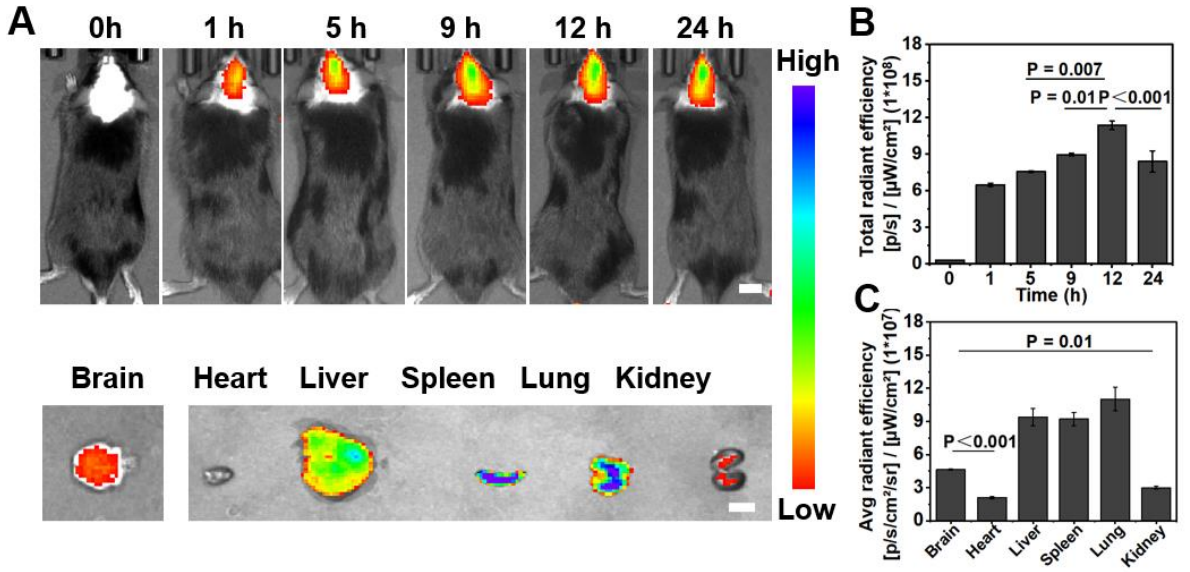

Figure S37. (A) *In vivo* fluorescence imaging of PD mice administrated with Cy5-labeled MSC EVs@MSeN-DT at different time points. The corresponding quantitative analysis of (B) the brain and (C) major organs form normal and PD mice treated by MSC EVs@MSeN-DT after 24 h intravenous injection (n = 3, Scale bar: 1 cm). All statistical data are presented as mean ± standard deviation. Statistical analysis: one-way ANOVA followed by Tukey's HSD post hoc test.

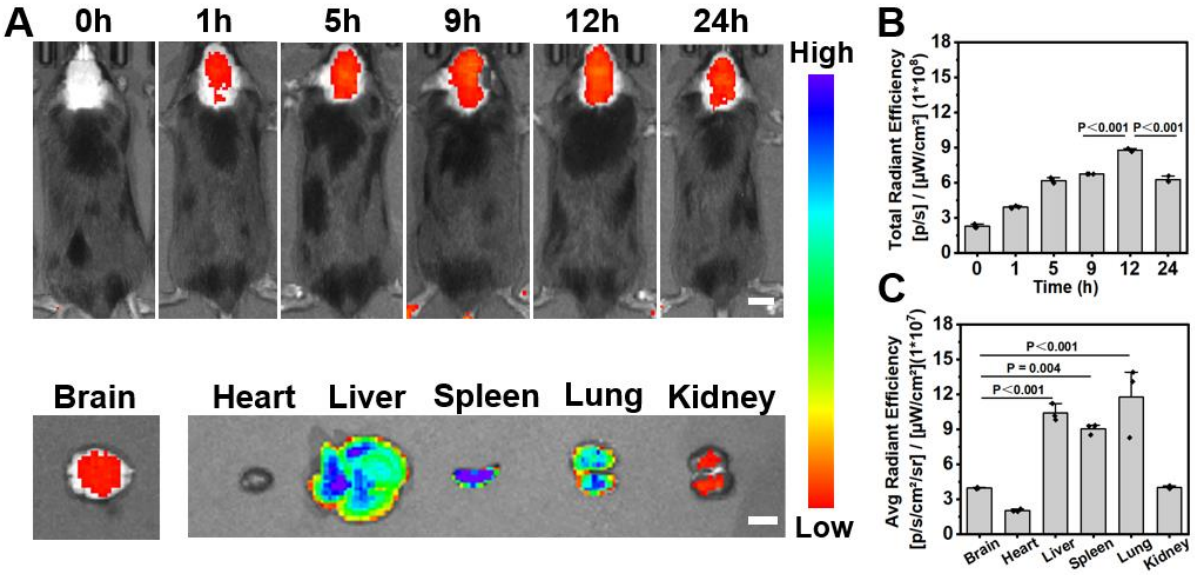

Figure S38. (A) *In vivo* fluorescence imaging of PD mice administrated with Cy5-labeled BEVs@MSeN-DT at different time points. The corresponding quantitative analysis of (B) the brain and (C) major organs form normal and PD mice treated by BEVs@MSeN-DT after 24 h intravenous injection (n = 3, Scale bar: 1 cm). All statistical data are presented as mean ± standard deviation. Statistical analysis: one-way ANOVA followed by Tukey's HSD post hoc test.

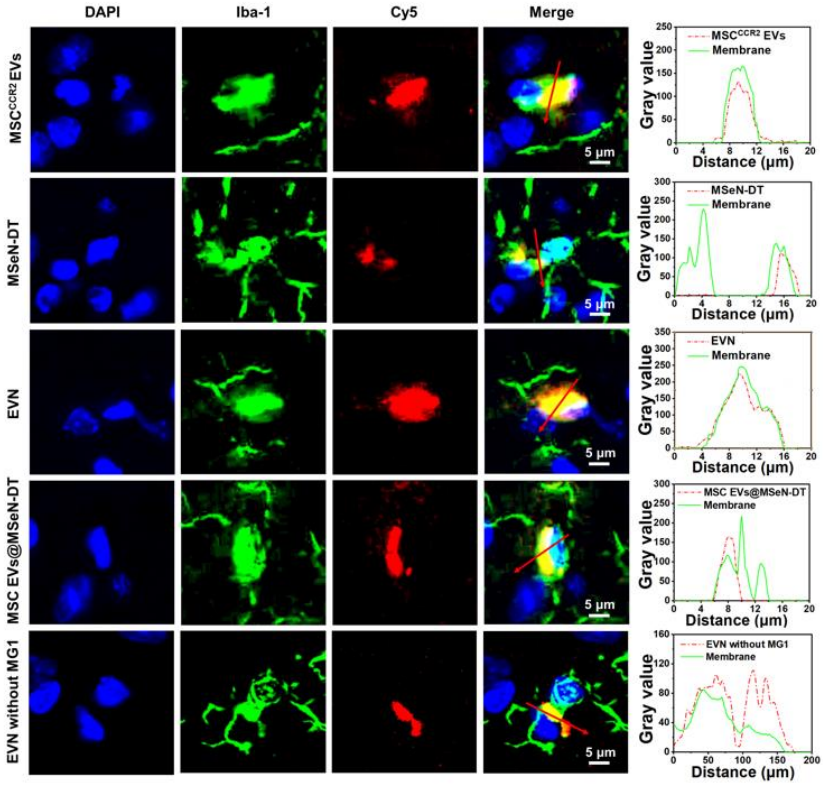

Figure S39. Representative co-localization immunofluorescence images in the brain of a PD mouse model after injection of Cy5-labeled different samples (blue: DAPI; green: microglia Iba-1; red: Cy5-labeled sample).

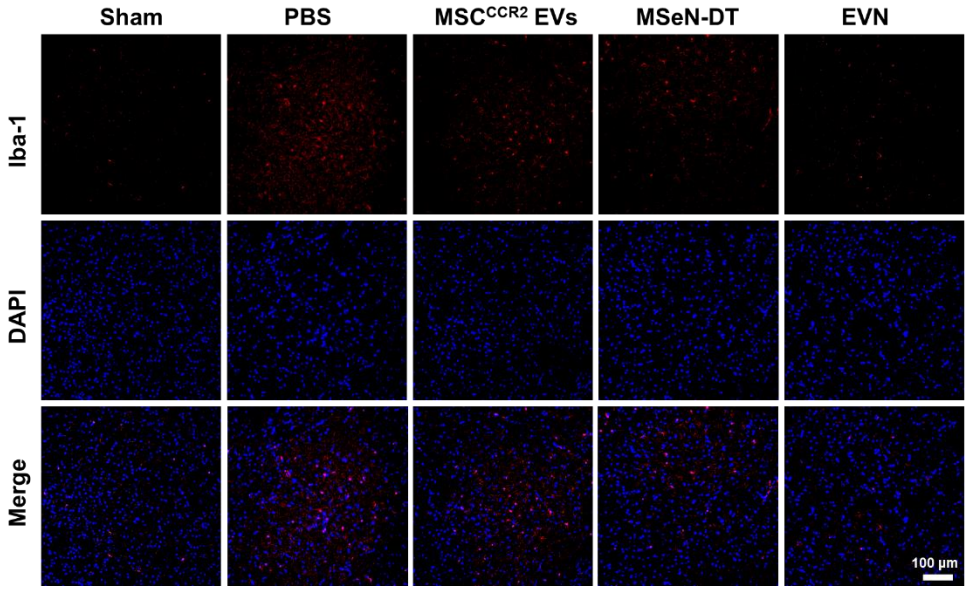

Figure S40. Immunofluorescence staining of Iba-1 (red) and DAPI (blue) in the SN of mice by different treatment.

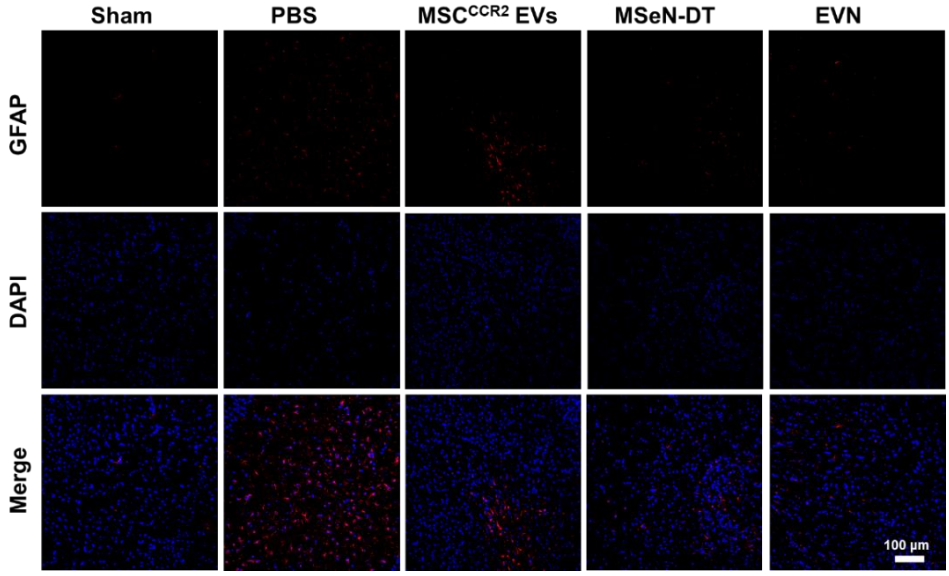

Figure S41. Immunofluorescence staining of GFAP (red) and DAPI (blue) in the SN of mice by different treatment.

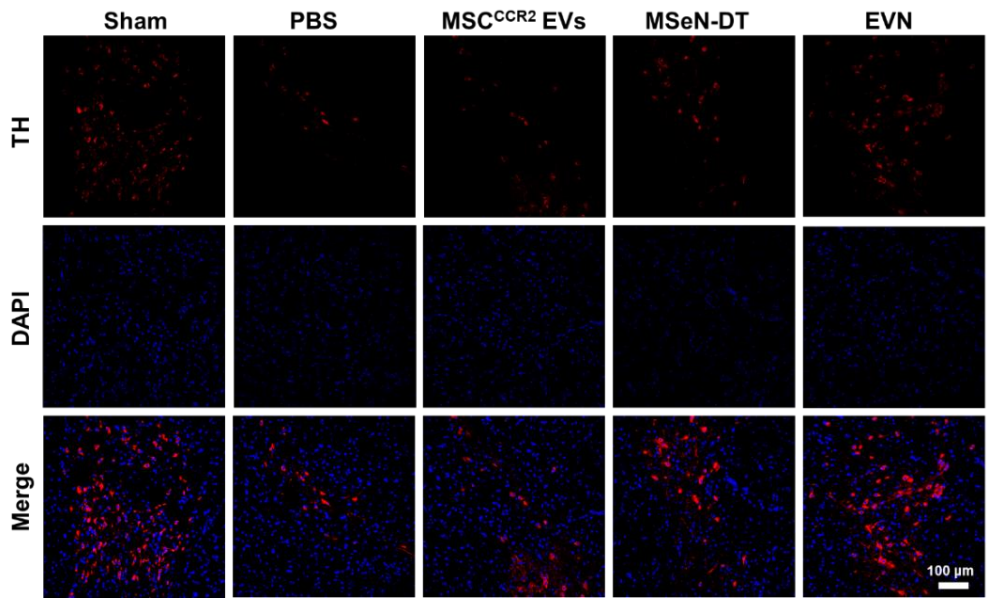

Figure S42. Immunofluorescence staining of TH (red) and DAPI (blue) in the SN of mice by different treatment.

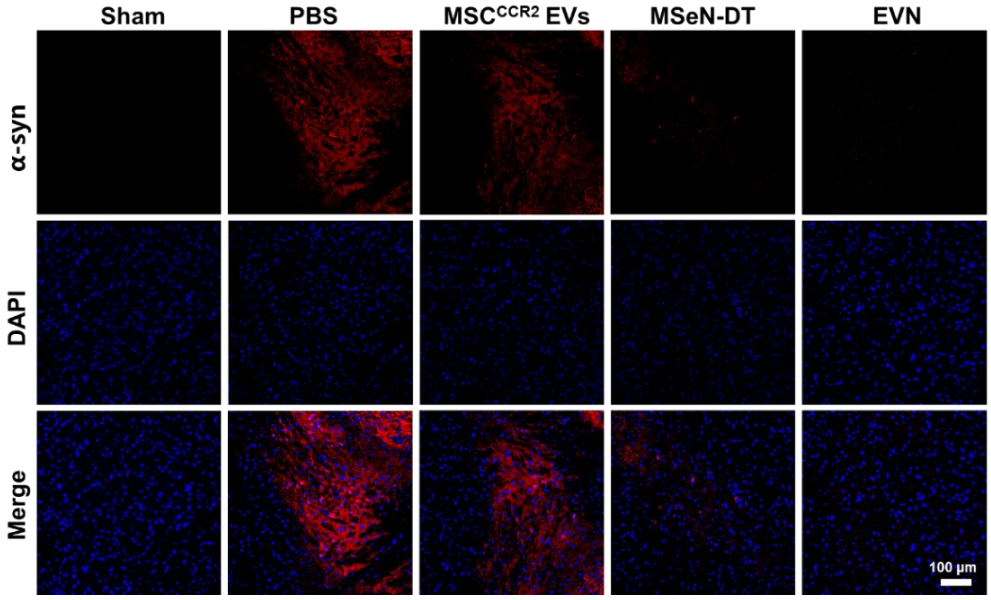

Figure S43. Immunofluorescence staining of α-syn (red) and DAPI (blue) in the SN of mice by different treatment.

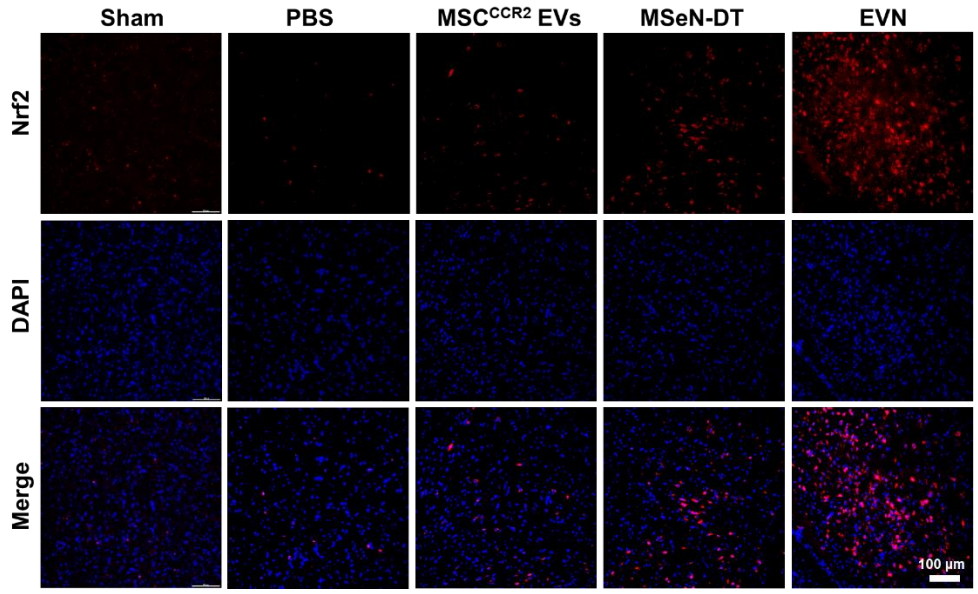

Figure S44. Immunofluorescence staining of Nrf2 (red) and DAPI (blue) in the SN of mice by different treatment.

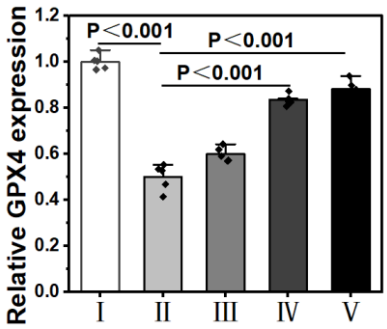

Figure S45. Quantitative analysis of GPX4 in the brain of mice by different treatment, in which the relative expression of GPX4 for the sham group was denoted as 1 (n = 5). (I: sham, II: PBS, III: MSC^{CCR2} EVs, IV: MSeN-DT, V: EVN). All statistical data are presented as mean ± standard deviation. Statistical analysis: one-way ANOVA followed by Tukey's HSD post hoc test.

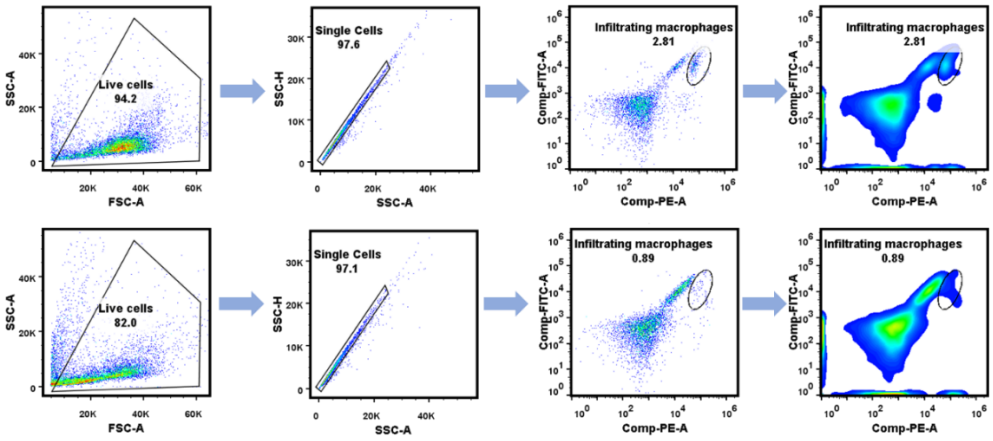

Figure S46. Gating strategy for CD45^{high} CD11b^{+} cells analysis in brain. The perfused brain tissues were digested and the dissociated cells were collected for flow cytometry analysis to examine the macrophages cells. 100,00 events were collected for each sample in the analysis. Live cells were chosen based on size in the FSC/SSC plots, and then singel cells number was determined by SSCA/SSCH. On this basis, macrophages were selected by CD45^{high} CD11b^{+} gated sorting, which was presented on Figure 7H and 7I.

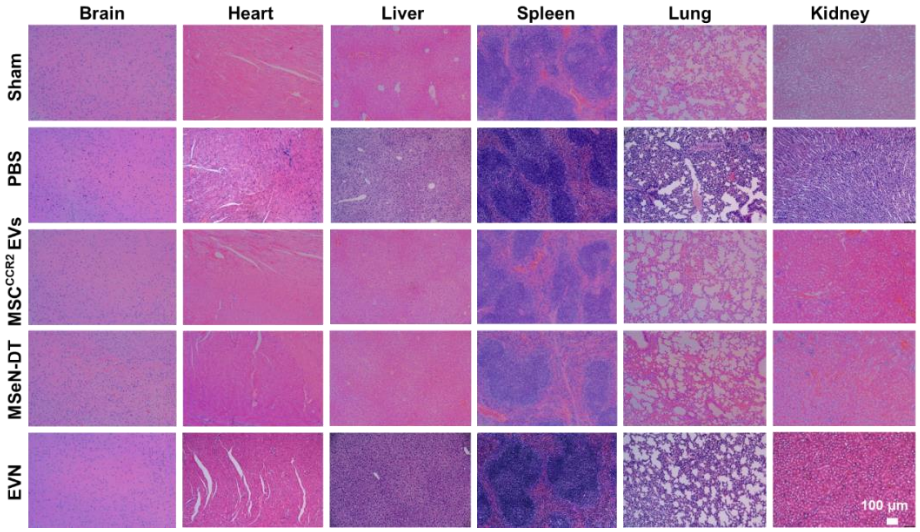

Figure S47. H&E staining images of brain and major organs, including the heart, liver, spleen, lung and kidney from the different groups of mice.

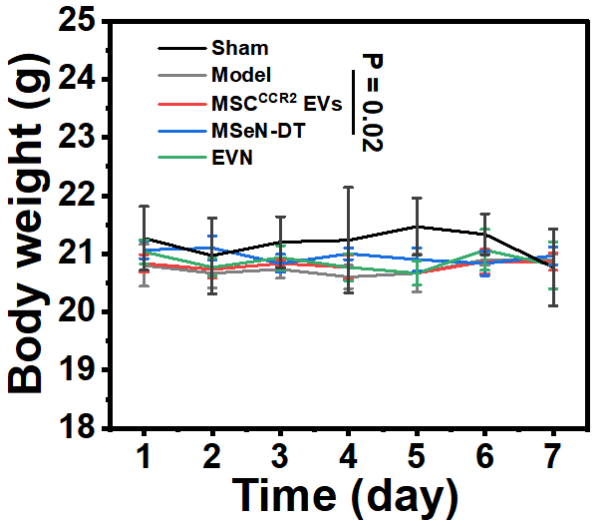

Figure S48. The body weight of mice treated by different samples during treatment (n = 3). Statistical analysis: two-way ANOVA followed by Tukey's multiple comparisons post test.

Table S1. Physicochemical properties of MSeN.

Samples	S_{BET} (m^2g^{-1}, C)	V ($cm^3 g^{-1}$)	D (nm)
MSeN	490.05	1.09	8.92

Table S2. Parameters and coefficients obtained for Zero order release kinetic model $Q_t=K_0t$, First order release kinetic model $ln\ (Q_0-Q_t) = lnQ_0-K_1t$ and Peppas release kinetic model $M_t/M_\infty = a \cdot t_b$ fitted to the DT release profiles from MseN-DT and EVN.

Sample	Release kinetic model	Release parameters	H_2O_2-	H_2O_2+
MSeN-DT	Zero-order	K_0	0.0465	0.4388
		R^2	0.8247	0.5146
	First-order	K_1	0.0238	0.0296
		R^2	0.9400	0.8118
	Peppas	a	0.1527	0.3456
		b	0.4073	0.2497
		R^2	0.9705	0.8395
EVN	Zero-order	K_0	0.0210	0.4227
		R^2	0.5073	0.4233
	First-order	K_1	0.0267	0.0339
		R^2	0.8327	0.8040
	Peppas	a	0.3080	0.3512
		b	0.2735	0.2507
		R^2	0.8504	0.8172

Table S3. Element content of EVN by TEM-mapping.

Element	Atomic Fraction (%)	Atomic Error (%)
O	69.37	3.66
Si	27.37	3.82
Se	1.76	0.26
P	1.5	0.34

Table S4. Blood routine analysis of mice after being treated with different samples.

Group	Sham	Model	MSC^{CCR2} EVs	MSeN-DT	EVN
Leukocyte count	9.2	9.8	10.9	9.6	9.7
Neutrophil count	1.6	2.0	2.0	2.5	1.5
Lymphocyte	7.4	7.5	8.6	6.4	7.8
Red blood cell count（RBC）	8.55	8.94	7.90	8.02	6.50
Hemoglobin (HGB)	135	138	125	138	120
Hematocrit (HCT)	41.2	42.1	39.5	34.2	32.1
Mean corpuscular volume (MCV)	48.2	47.2	50.1	42.7	49.5
Mean hemoglobin content (MCH)	15.7	15.4	15.8	17.2	18.4
Average hemoglobin concentration (MCHC)	327	327	316	403	373
RBC volume distributing width (RDW)	14.5	14.4	16.4	35.4	30.8

Table S5. Summary of current nanotherapeutic for remodeling the brain immune microenvironment of PD.

Sample	Inflammatory			Immune homeostasis			Ref.
	a	b	c	d	e	f	
mPDAN	melatonin	PI3K/Akt	N	×	×	×	5
PtCu	PtCu	nanozymes	N	×	×	×	6
CSPQ@CM	$Cu_{2-x}Se$-Qe	Bcl-2 and caspase-3	N	×	×	×	7
REXO-C/ANP/S	curcumin	×	N	imDC EXO	inhibiting T_{H17} differentiation and promoting T_{reg} production	inhibiting immune activation	8
Lf-Au-Bi_2Se_3	Au-Bi_2Se_3	multiple enzymes	N	×	×	×	9
MAG-NCs@Gel	magnolol	×	N	×	×	×	10
AL-GA-NGTH	AL-GA-NG	PI3K/Akt	N	×	×	×	11
RVG29-RBCm/Cur	curcumin	×	N	×	×	×	12
L.p@L30D-55	GABA	p38MAPK/NF-κB	N	×	×	×	13
PR-EXO/PP@Cur	curcumin	×	N	PR-EXO	restoring the number of T_{reg}	inhibiting immune activation	14
CN-hemin	CN-hemin	multiple enzymes	N	×	×	×	15
Fe-Cur	Fe-Cur	×	N	×	×	×	16
PBzyme	PBzyme	NLRP3-caspase1-GSDMD	N	×	×	×	17
PDASeCys	selenocystine	multiple enzymes	N	×	×	×	18
MSCEXO/PMAS/Ce-PABMS	NO	MMP-2	Y	×	×	×	19
	CeO_2	nanozymes	N	×	×	×	20
LSLGMA	siRNA	NF-κB	N	×	×	×	21
DTD-RM	rasagiline mesylate	×	N	×	×	×	22
Ptzyme@D-ZIF	Ptzyme	GPX4	N	×	×	×	23
Lf-UZSP	Pae	×	N	×	×	×	24
PDA-AFn	PDA-AFn	×	N	×	×	×	25
BLIPO-CUR	curcumin	×	N	×	×	×	26
ZAAM	NBC	×	N	×	×	×	27
MOF@Man	MOF@Man	NLRP3	N	×	×	×	28
CSCCT NPs	curcumin	SIRT1/PGC-1α	Y	×	×	×	29
CSPQ	quercetin	Nrf2-SQSTM1/p62	Y	×	×	×	30
NanoQC	quercetin	NLRP	N	×	×	×	31
RVG29@AHM@Pt/CeO_2	Pt/CeO_2	nanozymes /mitophagy	Y	×	×	×	32
TPP-rHuHF-LYC	TPP-rHuHF-LYC	PINK1/parkin	Y	×	×	×	33

HSA/Se NPs	HSA/Se NPs	Keap1-Nrf2-SOD	Y	×	×	×	34
QPMP	Que/Ptzyme	×	N	×	×	×	35
AA-IONPS	Ascorbic acid	×	N	×	×	×	36
RNP-DFO	DFO	iron chelation	N	×	×	×	37
PCM	PCM	×	Y	×	×	×	38
EVN	DT	Nrf2-GPX4	Y	MCS^{CCR2} EVs	blocking of the CCR2-CCL2 axis	inhibiting the infiltration of peripheral inflammatory cell	This work

[a]Anti-inflammatory material or durg
[b]Anti-inflammatory pathway
[c]Whether ROS is inhibited from upstream (Y represented Yes, N represented NO)
[d]Regulatory material or drug
[e]Regulatory pathway
[f]Purpose of Regulation

Table S6. Summary of current research models of nanotherapeutic for cell infiltration mediated by chemokine in disease treatment.

Sample	Chemokine	Chemotaxis	Purpose	Disease	Research model							Ref.
					In vitro				In vivo			
					a	b	c	d	e	f	g	
Au NPs	CCR5	×	Delaying macrophages wound response	Tissue damage	×	×	√	×	×	√	√	39
mNOX-E36	CCR2	CCR2-CCL2	Blocking macrophage infiltration	Breast cancer	×	×	×	×	√	×	√	40
DNA/dendrimer	CCL20	CCR6-CCL20	Reducing the neuroinflammation	Traumatic brain injury	×	×	×	×	√	×	×	41
Fe_3O_4@Pt@E5	CXCR4	CXCR4/CXCL12	Inhibiting the growth, adhesion and infiltration of leukemia cells	Acute myeloid leukemia	×	×	×	√	√	√	√	42
S@PBMHA	CXCL12	CXCR4/CXCL12	Recruiting BMSCs to bone defect areas	Bone defects	×	×	√	×	×	×	√	43
CXCL12-NPs	CXCL12	CXCR4/CXCL12	Decreasing $CXCR4^+$-cell migration	Cancer	×	×	√	√	×	×	×	44
BPL/rGO	CXCL12	CXCR4/CXCL12	Increasing distribution to CXCR4-positive tumors	Tumor	×	×	×	√	√	×	×	45
NPTyr-C9AP	CXCL9	CXCR3/CXCL9	T-cell recruitment	Melanoma	×	×	√	√	×	√	√	46
DEX-N-NVs	CCR2、CXCR2、CXCR4	×	Enhancing retention and targeting to activated macrophages and DCs	COVID-19	×	×	×	√	×	×	√	47
liposome-protamine-DNA	CXCL12	CXCR4/CXCL12	Enhancing the activation of tumor-infiltrating DCs and NK cells, and increasing active T-cell infiltration	Cancer	×	×	×	×	√	×	√	48
lipid-protamine-DNA (LPD)	CXCL12	CCR7/CCL21	Inhibiting TNBC lymphatic metastasis	Breast cancer	×	×	√	×	√	√	√	49
M-E5	CXCL12	CXCR4/CXCL12	Inhibiting the engraftment of AML cells in BM and spleen	Acute myeloid leukemia	√	×	√	×	×	×	√	50
CCR2-MM@PLGA/Cur/NPs	CCR2	CCR2-CCL2	Targeting/attenuated macrophage infiltration	Spinal cord injury	√	×	√	√	√	×	×	51

MCSNs	CXCR4	CXCR4/ SDF-1	Targeting/promoting evasion of immune cells	Tumor	×	×	√	√	×	×	×	52
FV@CX5461	CCR6	CCR6-CCL20	Targeting/ induce Treg cell infiltration	Autoimmune skin disorders	×	×	√	×	√	×	√	53
AM3100SPNPS	CXCL12	CXCL12/CXCR4	Reducing infiltration of CXCR4+ monocytic myeloid-derived suppressor cells	Glioblastoma	×	×	√	×	√	×	√	54
EVN	CCR2	CCR2-CCL2	Targeting/inhibiting inflammatory cell infiltration	Parkinson's disease	√	√	√	√	√	√	√	This work

[a]representing study of the ability to bond chemokines under static conditions *in vitro*;
[b]representing study of chemotactic behavior under dynamic conditions *in vitro*;
[c]representing study of cell infiltration mediated by chemokine *in vitro*;
[d]representing study of chemotaxis to target cells *in vitro*;
[e]representing study of chemotactic behavior *in vivo*;
[f]representing study of chemotaxis to target cells *in vivo*;
[g]representing study of cell infiltration mediated by chemokine *in vivo*.

References

(1) Kuang, S.; He, F.; Liu, G.; Sun, X.; Dai, J.; Chi, A.; Tang, Y.; Li, Z.; Gao, Y.; Deng, C.; Lin, Z.; Xiao, H.; Zhang, M. CCR2-engineered mesenchymal stromal cells accelerate diabetic wound healing by restoring immunological homeostasis. *Biomaterials* **2021**, *275*, 0142-9612.

(2) Yin, N.; Zhao, Y.; Liu, C.; Yang, Y.; Wang, Z. H.; Yu, W.; Zhang, K.; Zhang, Z.; Liu, J.; Zhang, Y.; Shi, J. Engineered nanoerythrocytes alleviate central nervous system inflammation by regulating the polarization of inflammatory microglia. *Adv. Mater.* **2022**, *34*, 2201322.

(3) Shao, D.; Zhang, F.; Chen, F.; Zheng, X.; Hu, H.; Yang, C.; Tu, Z.; Wang, Z.; Chang, Z.; Lu, J.; Li, T.; Zhang, Y.;Chen, L.; Leong, K. W.; Dong, W. F. Biomimetic diselenide-bridged mesoporous organosilica nanoparticles as an x-ray-responsive biodegradable carrier for chemo-immunotherapy. *Adv. Mater.* **2020**, *32*, e2004385.

(4) Liu, Y.Q.; Mao, Y.; Xu, E.; Jia, H.; Zhang, S.; Dawson, V. L.; Dawson, T. M.; Li, Y.M.; Zheng, Z.; He, W.; Mao, X. Nanozyme scavenging ROS for prevention of pathologic α-synuclein transmission in Parkinson's disease. *Nano Today* **2021**, *36*, 1748-0132.

(5) Aday, S.; Li, W.; Karp, J. M.; Joshi, N. An in vitro blood-brain barrier model to study the penetration of nanoparticles. *Bio. Protoc.* **2022,** *12*, e4334.

(6) Srivastava, A. K.; Roy Choudhury, S.; Karmakar, S. Melatonin/polydopamine nanostructures for collective neuroprotection-based Parkinson's disease therapy. *Biomater. Sci.* **2020,** *8*, 1345-1363.

(7) Liu, H.; Han, Y.; Wang, T.; Zhang, H.; Xu, Q.; Yuan, J.; Li, Z. Targeting microglia for therapy of Parkinson's disease by using biomimetic ultrasmall nanoparticles. *J. Am. Chem. Soc.* **2020,** *142*, 21730-21742.

(8) L. Liu, Y. Li, H. Peng, R. Liu, W. Ji, Z. Shi, J. Shen, G. Ma, X. Zhang. Targeted exosome coating gene-chem nanocomplex as "nanoscavenger" for clearing α-synuclein and immune activation of Parkinson's disease. *Sci. Adv.* **2020**, *6*, eaba3967.

(9) Li, L.; Lu, Y.; Xu, X.; Yang, X.; Chen, L.; Jiang, C.; Wang, Y.; Hu, W.; Wei, X.; Yang, Z. Catalytic-enhanced lactoferrin-functionalized Au-Bi_2Se_3 nanodots for Parkinson's disease therapy via reactive oxygen attenuation and mitochondrial protection. *Adv. Healthc. Mater.* **2021,** *10*, e2100316.

(10) Tan, Y.; Liu, Y.; Liu, Y.; Ma, R.; Luo, J.; Hong, H.; Chen, X.; Wang, S.; Liu, C.; Zhang, Y.; Chen, T. Rational design of thermosensitive hydrogel to deliver nanocrystals with intranasal administration for brain targeting in Parkinson'sdisease. *Research* **2021,** *2021*, 9812523.

(11) Chen, Y.B.; Qiao, T.; Wang, Y.Q.; Cui, Y.L.; Wang, Q.S. Hydrogen bond-enhanced nanogel delivery system for potential intranasal therapy of Parkinson's disease. *Mater. Design* **2022,** *219*, 0264-1275.

(12) Liu, Y.; Luo, J.; Liu, Y.; Liu, W.; Yu, G.; Huang, Y.; Yang, Y.; Chen, X.; Chen, T. Brain-targeted biomimetic nanodecoys with neuroprotective effects for precise therapy of Parkinson's disease. *ACS Cent. Sci.* **2022,** *8*, 1336-1349.

(13) Guo, M.; Yang, C.; Li, B.; Cheng, S. X.; Guo, Q.; Ming, D.; Zheng, B. Bionic dormant body of timed wake-up for bacteriotherapy in Vivo. *ACS Nano* **2022,** *16*, 823-836.

(14) Peng, H.; Li, Y.; Ji, W.; Zhao, R.; Lu, Z.; Shen, J.; Wu, Y.; Wang, J.; Hao, Q.; Wang, J.; Wang, W.; Yang, J.; Zhang, X. Intranasal administration of self-oriented nanocarriers based on therapeutic exosomes for synergistic treatment of Parkinson's disease. *ACS Nano* **2022,** *16*, 869-884.

(15) Lei, L.; Tu, Q.; Jiao, L.; Xiang, S.; Wang, L.; Ran, X.; Xiao, B.; Feng, G.; Feng, J.; Zhang, C. Reactive oxygen species scavenging by hemin-based nanosheets reduces Parkinson's disease symptoms in an animal model. *Chem. Eng. J.* **2022,** *432*, 1385-8947.

(16) Cheng, G.; Liu, X.; Liu, Y.; Liu, Y.; Ma, R.; Luo, J.; Zhou, X.; Wu, Z.; Liu, Z.; Chen, T.; Yang, Y. Ultrasmall coordination polymers for alleviating ROS-mediated inflammatory and realizing neuroprotection against Parkinson's disease. *Research* **2022,** *2022*, 9781323.

(17) Ma, X.; Hao, J.; Wu, J.; Li, Y.; Cai, X.; Zheng, Y. Prussian blue nanozyme as a pyroptosis inhibitor alleviates neurodegeneration. *Adv. Mater.* **2022,** *34*, e2106723.

(18) Wang, W.; Zheng, J.; Zhou, H.; Liu, Q.; Jia, L.; Zhang, X.; Ge, D.; Shi, W.; Sun, Y. Polydopamine-based nanocomposite as a biomimetic antioxidant with a variety of enzymatic activities for Parkinson's disease. *ACS Appl. Mater. Interfaces* **2022,** *14*, 32901-32913.

(19) Wang, Q.; Li, T.; Yang, J.; Zhao, Z.; Tan, K.; Tang, S.; Wan, M.; Mao, C. Engineered exosomes with independent module/ccascading function for therapy of Parkinson's disease by multistep targeting and multistage intervention method. *Adv. Mater.* **2022,** *34*, e2201406.

(20) Ji, W.; Li, Y.; Peng, H.; Zhao, R.; Shen, J.; Wu, Y.; Wang, J.; Hao, Q.; Lu, Z.; Yang, J.; Zhang, X. Self-catalytic small interfering RNA nanocarriers for synergistic treatment of neurodegenerative diseases. *Adv. Mater.* **2022,** *34*, e2105711.

(21) Wu, Y.; Wang, W.; Qiu, X.; Lu, Z.; Ji, W.; Shen, J.; Peng, H.; Zhao, R.; Wang, J.; Zhang, T.; Yang, J.; Zhang, X. A STIR nucleic acid drug delivery system for stirring phenotypic switch of microglia in Parkinson's disease treatments. *Nano Res.* **2023,** *16*, 7216-7226.

(22) Fan, Z.; Jin, H.; Tan, X.; Li, Y.; Shi, D.; Wang, Q.; Meng, J.; Li, W.; Chen, C.; Peng, L.; Hou, Z.; Li, J.; Jin, X.; Yang, L. ROS-responsive hierarchical targeting vehicle-free nanodrugs for three-pronged Parkinson's disease therapy. *Chem. Eng. J.* **2023,** *466*, 1385-8947.

(23) Jiang, W.; Li, Q.; Zhang, R.; Li, J.; Lin, Q.; Li, J.; Zhou, X.; Yan, X.; Fan, K. Chiral metal-organic frameworks incorporating nanozymes as neuroinflammation inhibitors for managing Parkinson's disease. *Nat. Commun.* **2023,** *14*, 8137.

(24) Hu, B.; Fang, H.; Huang, Z.; Huang, W.; Huang, L.; Liu, H.; Lv, F.; Huang, W.; Wang, X. An upconversion nanoplatform based multi-effective theatment for Parkinson's disease. *Chem. Eng. J.* **2023,** *465*, 1385-8547.

(25) Yao, K.; Gan, J.; Zhao, D.; Li, M.; Shen, X.; Yang, Y.; Feng, P.; Shen, Q. A core-satellite-like nanoassembly reverses a decisive tyrosine hydroxylase loss in degenerative dopaminergic neurons. *Nano Res.* **2023,** *16*, 9835-9847.

(26) Liu, J.; Gao, D.; Hu, D.; Lan, S.; Liu, Y.; Zheng, H.; Yuan, Z.; Sheng, Z. Delivery of biomimetic liposomes via meningeal lymphatic vessels route for targeted therapy of Parkinson's disease. *Research* **2023,** *6*, 0030.

(27) Sun, Y.; Kong, J.; Ge, X.; Mao, M.; Yu, H.; Wang, Y. An antisense oligonucleotide-loaded blood-brain barrier penetrable nanoparticle mediating recruitment of endogenous neural stem cells for the treatment of Parkinson's disease. *ACS Nano* **2023,** *17*, 4414-4432.

(28) Li, Q.; Ding, X.; Chang, Z.; Fan, X.; Pan, J.; Yang, Y.; Li, X.; Jiang, W.; Fan, K. Metal-organic framework based nanozyme system for NLRP3 inflammasome-mediated neuroinflammatory regulation in Parkinson's disease. *Adv. Healthc. Mater.* **2023**, *13*, e2303454.

(29) Zheng, Q.; Liu, H.; Zhang, H.; Han, Y.; Yuan, J.; Wang, T.; Gao, Y.; Li, Z. Ameliorating mitochondrial dysfunction of neurons by biomimetic targeting nanoparticles mediated mitochondrial biogenesis to boost the therapy of Parkinson's disease. *Adv. Sci.* **2023,** *10*, e2300758.

(30) Liu, H.; Zheng, Q.; Yuan, J.; Gao, Y.; Wang, T.; Zhang, H.; Li, Z. Modulating SQSTM1/p62-dependent selective autophagy of neurons by activating Nrf2 with multifunctional nanoparticles to eliminate α-synuclein aggregates and boost therapy of Parkinson's disease. *Nano Today* **2023,** *49*, 101770.

(31) Zhao, D.; Tian, C.; Cheng, M.; Yang, F.; Tian, C.; Liu, Y.; Chen, Z.; Pang, G.; Shen, H.; Chang, J.; Dou, Y. Carrier-free quercetin nanomedicine blocks NLRP3 deubiquitination and TXNIP recruitment for Parkinson's disease therapy. *Chem. Eng. J.* **2023,** *464*, 1385-8947.

(32) Li, B.; Bai, Y.; Yion, C.; Wang, H.; Su, X.; Feng, G.; Guo, M.; Peng, W.; Shen, B.; Zheng, B. Single-atom nanocatalytic therapy for suppression of neuroinflammation by inducing autophagy of abnormal mitochondria. *ACS Nano* **2023,** *17*, 7511-7529.

(33) Xia, X.; Li, H.; Xu, X.; Zhao, G.; Du, M. Facilitating pro-survival mitophagy for alleviating Parkinson's disease via sequence-targeted lycopene nanodots. *ACS Nano* **2023,** *17*, 17979-17995.

(34) Xu, K.; Huang, P.; Wu, Y.; Liu, T.; Shao, N.; Zhao, L.; Hu, X.; Chang, J.; Peng, Y.; Qu, S. Engineered selenium/human serum albumin nanoparticles for efficient targeted treatment of Parkinson's disease via oral gavage. *ACS Nano* **2023,** *17*, 19961-19980.

(35) Li, Q.; Wu, T.; Akakuru, O. U.; Song, N.; Liu, W.; Jiang, W.; Fan, K. A dual synergetic nanoreactor for managing Parkinson's disease by regulating inflammation and mitigating oxidative damage. *Adv. Funct. Mater.* **2023,** *33*, 2214826.

(36) Li, L.; Luo, P.; Wu, S.; Wang, Y. Deciphering the neuroprotective effect of ascorbic acid mediated synthesis of iron oxide nanoparticles against Parkinson's disease: an in vitro and in vivo approach. *Macromol. Res.* **2023,** *31*, 949-960.

(37) You, L.; Wang, J.; Liu, T.; Zhang, Y.; Han, X.; Wang, T.; Guo, S.; Dong, T.; Xu, J.; Anderson, G. J.; Liu, Q.; Chang, Y. Z.; Lou, X.; Nie, G. Targeted brain delivery of rabies virus glycoprotein 29-modified deferoxamine-loaded nanoparticles reverses functional deficits in parkinsonian mice. *ACS Nano* **2018,** *12*, 4123-4139.

(38) Zhao, Z.; Chen, L.; Yang, C.; Guo, W.; Huang, Y.; Wang, W.; Wan, M.; Mao, C.; Shen, J. Nanomotor-based H_2S donor with mitochondrial targeting function for treatment of Parkinson's disease. *Bioact. Mater.* **2024,** *31*, 578-589.

(39) Xu, J.; Wang, J.; Qiu, J.; Liu, H.; Wang, Y.; Cui, Y.; Humphry, R.; Wang, N.; DurKan, C.; Chen, Y.; Lu, Y.; Ma, Q.; Wu, W.; Luo, Y.; Xiao, L.; Wang, G. Nanoparticles retard immune cells recruitment in vivo by inhibiting chemokine expression. *Biomaterials* **2021,** *265*, 120392.

(40) Mockel, D.; Bartneck, M.; Niemietz, P.; Wagner, M.; Ehling, J.; Rama, E.; Weiler, M.; Gremse, F.; Eulberg, D.; Pola, R.; Pechar, M.; Etrych, T.; Storm, G.; Kiessling, F.; Tacke, F.; Lammers, T. CCL2 chemokine inhibition primes the tumor vasculature for improved nanomedicine delivery and efficacy. *J. Control Release* **2023,** *365*, 358-368.

(41) Mayilsamy, K.; Markoutsa, E.; Das, M.; Chopade, P.; Puro, D.; Kumar, A.; Gulick, D.; Willing, A. E.; Mohapatra, S. S.; Mohapatra, S. Treatment with shCCL20-CCR6 nanodendriplexes and human mesenchymal stem cell therapy improves pathology in mice with repeated traumatic brain injury. *Nanomedicine* **2020,** *29*, 102247.

(42) Kong, F.; Bai, H.; Ma, M.; Wang, C.; Xu, H.; Gu, N.; Zhang, Y. Fe_3O_4@Pt nanozymes combining with CXCR4 antagonists to synergistically treat acute myeloid leukemia. *Nano Today* **2021,** *37*, 101106.

(43) Wei, J.; Xia, X.; Xiao, S.; Jin, S.; Zou, Q.; Zuo, Y.; Li, Y.; Li, J. Sequential dual-biofactor release from the scaffold of mesoporous HA microspheres and PLGA matrix for boosting endogenous bone regeneration. *Adv. Healthc. Mater.* **2023,** *12*, e2300624.

(44) Pisani, A.; Donno, R.; Gennari, A.; Cibecchini, G.; Catalano, F.; Marotta, R.; Pompa, P. P.; Tirelli, N.; Bardi, G. CXCL12-PLGA/Pluronic nanoparticle internalization abrogates CXCR4-mediated cell migration. *Nanomaterials* **2020,** *10*, 2304.

(45) Ko, S.; Shim, G.; Kim, J.; Oh, Y.K. Chemokine-mimetic plerixafor derivative for tumor-specific delivery of nanomaterials. *Nano Res.* **2018,** *11*, 2159-2172.

(46) Wang, Y.; Zhou, S. K.; Wang, Y.; Lu, Z. D.; Zhang, Y.; Xu, C. F.; Wang, J. Engineering tumor-specific gene nanomedicine to recruit and activate T cells for enhanced immunotherapy. *Nat. Commun.* **2023,** *14*, 1993.

(47) Meng, Q. F.; Tai, W. B.; Tian, M. Y.; Zhuang, X. Y.; Pan, Y. W.; Lai, J. L.; Xu, Y.T.; Xu, Z. Q.; Li, M.; Zhao, G. Y.; Yu, G. T.; Yu, G. C.; Chen, R. C.; Jin, N. Y.; Li, X.; Cheng, G.; Chen, X. Y.; Rao, L. Inhalation delivery of dexamethasone with iSEND nanoparticles attenuates the COVID-19 cytokine storm in mice and nonhuman primates. *Sci. Adv.* **2023,** *9*, eadg3277.

(48) Shen, L.; Li, J.; Liu, Q.; Song, W.; Zhang, X.; Tiruthani, K.; Hu, H.; Das, M.; Goodwin, T. J.; Liu, R.; Huang, L. Local blockade of interleukin 10 and C-X-C motif chemokine ligand 12 with nano-delivery promotes antitumor response in murine cancers. *ACS Nano* **2018,** *12*, 9830-9841.

(49) An, S.; Tiruthani, K.; Wang, Y.; Xu, L.; Hu, M.; Li, J.; Song, W.; Jiang, H.; Sun, J.; Liu, R.; Huang, L. Locally trapping the C-C chemokine receptor type 7 by gene delivery nanoparticle inhibits lymphatic metastasis prior to tumor resection. *Small* **2019,** *15*, e1805182.

(50) Meng, J.; Ge, Y.; Xing, H.; Wei, H.; Xu, S.; Liu, J.; Yan, D.; Wen, T.; Wang, M.; Fang, X.; Ma, L.; Yang, Y.; Wang, C.; Wang, J.; Xu, H. Synthetic CXCR4 antagonistic peptide assembling with nanoscaled micelles combat acute myeloid leukemia. *Small* **2020,** *16*, e2001890.

(51) Gu, C.; Geng, X.; Wu, Y.; Dai, Y.; Zeng, J.; Wang, Z.; Fang, H.; Sun, Y.; Chen, X. Engineered macrophage membrane-coated nanoparticles with enhanced CCR2 expression promote spinal cord injury repair by suppressing neuroinflammation and neuronal death. *Small* **2023**, *20*, e2305659.

(52) Zou, D.; Wu, Z.; Yi, X.; Hui, Y.; Yang, G.; Liu, Y.; Tengjisi; Wang, H.; Brooks, A.; Wang, H.; Liu, X.; Xu, Z. P.; Roberts, M. S.; Gao, H.; Zhao, C. X. Nanoparticle elasticity regulates the formation of cell membrane-coated nanoparticles and their nano-bio interactions. *Proc. Natl. Acad. Sci. U. S. A.* **2023,** *120*, e2214757120.

(53) Huang, R.; Jia, B.; Su, D.; Li, M.; Xu, Z.; He, C.; Huang, Y.; Fan, H.; Chen, H.; Cheng, F. Plant exosomes fused with engineered mesenchymal stem cell-derived nanovesicles for synergistic therapy of autoimmune skin disorders. *J. Extracell. Vesicles* **2023,** *12*, e12361.

(54) Alghamri, M. S.; Banerjee, K.; Mujeeb, A. A.; Mauser, A.; Taher, A.; Thalla, R.; McClellan, B. L.; Varela, M. L.; Stamatovic, S. M.; Martinez-Revollar, G.; Andjelkovic, A. V.; Gregory, J. V.; Kadiyala, P.; Calinescu, A.; Jimenez, J. A.; Apfelbaum, A. A.; Lawlor, E. R.; Carney, S.; Comba, A.; Faisal, S. M.; et al. Systemic delivery of an adjuvant CXCR4-CXCL12 signaling inhibitor encapsulated in synthetic protein nanoparticles for glioma immunotherapy. *ACS Nano* **2022,** *16*, 8729-8750.